Proteome-wide Mendelian randomization implicates TIMP2 as a putative causal protein for bone mineral density and fracture risk

Chen-Yang Su[1–3], Maya Akerman[3,4], Masashi Hasebe[2,3,5,6], Satoshi Yoshiji[1–3,5,7*]

[1]Quantitative Life Sciences, McGill University, Montréal, Québec, Canada
[2]Victor Phillip Dahdaleh Institute of Genomic Medicine, McGill University, Montréal, Québec, Canada
[3]Canada Excellence Research Chair in Genomic Medicine, McGill University, Montréal, Québec, Canada
[4]Department of Biology, McGill University, Montréal, Québec, Canada
[5]Department of Human Genetics, McGill University, Montréal, Québec, Canada
[6]Department of Diabetes, Endocrinology and Nutrition, Kyoto University Graduate School of Medicine, Kyoto, Japan
[7]Programs in Metabolism and Medical & Population Genetics, The Broad Institute of MIT and Harvard, Cambridge, MA, USA

*Correspondence

Corresponding Author:
Satoshi Yoshiji, MD, PhD
Department of Human Genetics, McGill University
Address: 740 Dr Penfield Ave, Montréal, Québec, H3A 0G1, Canada
E-mail: satoshi.yoshiji@mcgill.ca
Phone: +1 (514) 398-3311

Abstract (300 words)

Osteoporosis is a highly prevalent cause of fractures in older adults and remains a critical source of morbidity that requires continued efforts to develop new therapeutics. Circulating proteins play a critical role in the pathophysiology of osteoporosis and offer opportunities to identify new putatively causal determinants of bone health. We therefore performed a large-scale proteome-wide Mendelian randomization (MR) analysis to systematically estimate the effects of genetically determined circulating proteins levels on bone mineral density (BMD) and fracture risk. Circulating proteins play critical role in osteoporosis pathophysiology and offer opportunities to identify new putative causal proteins of bone health, we performed large-scale proteome-wide Mendelian randomization (MR) to systematically estimate the effect of genetically determined circulating proteins levels on bone mineral density (BMD) and fracture risk. Genetic instruments were derived from *cis*-protein quantitative trait loci (*cis*-pQTLs) for 2,110 plasma proteins across four European ancestry cohorts and applied to genome-wide association studies (GWAS) of heel estimated BMD, femoral neck BMD, lumbar spine BMD, any fracture, and forearm fracture in up to 426,824 individuals of European ancestry. Across proteins and outcomes, 192 protein-outcome associations showed MR evidence of association and passed checks for weak instruments, heterogeneity, and horizontal pleiotropy, and 128 of these also showed strong colocalization with osteoporosis-related loci. We then prioritized proteins that replicated across cohorts, exhibited concordant effect directions, and were likely to be active in circulation, yielding 18 high-confidence causal proteins for BMD and fracture risk. These included established skeletal regulators such as sclerostin (SOST) and R-spondin-3 (RSPO3), which showed opposing effects consistent with their known biology, along with less well-characterized proteins. Among the latter, tissue inhibitor of metalloproteinases 2 (TIMP2) emerged as a particularly compelling candidate: higher genetically predicted TIMP2 levels were associated with lower BMD and increased forearm fracture risk. Gene-level and variant-level phenome-wide association analyses converged on musculoskeletal traits, and rare predicted damaging or loss-of-function variants in *TIMP2* were associated with higher BMD T-scores at the heel, spine and hip. Our findings implicate several circulating proteins as putatively causal factors for osteoporosis and, among them, provide multiple layers of evidence supporting TIMP2 as a potential therapeutic target.

Lay summary Max 100 words (aimed at a non-specialist audience)

Osteoporosis is characterized by decreased bone density, and despite available medications, it remains a key risk factor for fractures, requiring continued effort for development of new therapeutics. We used genetic data to estimate the effect of genetically predicted levels of 2,110 blood proteins on strength and fracture risk. We found 18 proteins with effects on bone mineral density and fractures. One protein, tissue inhibitor of metalloproteinases 2 (TIMP2), showed robust evidence linking its higher levels to decreased bone density and increased risk of forearm fracture, highlight TIMP2 as a promising new treatment target for osteoporosis.

Keywords 5–10 keywords

Mendelian randomization; proteomics; circulating proteins; bone mineral density; osteoporosis; fractures; TIMP2; SOST; RSPO3; drug targets

Introduction

Osteoporosis is a common age-related skeletal disorder characterized by decreased bone mineral density (BMD), leading to an increased risk of fractures. Globally, about 19.7% of adults meet WHO diagnostic criteria for osteoporosis[1]. Each year, an estimated 9 million fragility fractures occur worldwide, including roughly 1.6 million hip fractures, the most severe type of fracture[2]. These consequences are a major cause of chronic pain, disability, and mortality in older adults, and represent a substantial personal and socioeconomic burden. Although current therapies, including antiresorptive and anabolic agents, can reduce fracture risk, for example, bisphosphonates lower vertebral fractures by 50-70%, hip fractures by 40%, and non-vertebral fractures by 20-30%[3], substantial residual fracture risk remains. These limitations highlight the need for new therapeutic strategies informed by deeper mechanistic understanding of osteoporosis biology.

Circulating proteins are involved in diverse biological processes, and their dysregulation has been linked to many age-related diseases[4–6]. Recent evidence indicates that bone homeostasis, an essential process disrupted in osteoporosis, is also influenced by proteins in bloodstream[7]. Numerous circulating proteins have been associated with BMD and fracture risk in observational studies[8], but such findings are susceptible to residual confounding and reverse causation, limiting their ability to establish causal relationships. At the same time, circulating proteins represent attractive therapeutic targets because they are accessible to therapeutic modulation, including monoclonal antibodies, small molecules, or protein-based therapies. Their presence in blood also makes them suitable candidates for biomarker development for early disease detection, prognosis, and monitoring of treatment response[9,10].

Establishing causal relationships in human biology often requires approaches that can overcome the inherent limitations of observational studies. Mendelian randomization (MR) offers such an approach by using genetic variants as instrumental variables to infer causality[11]. Because genetic variants are randomly allocated at conception and remain fixed throughout life, MR is less susceptible to confounding and reverse causation. Recent advances in high-throughput proteomics and genome-wide association studies (GWAS) have enabled proteome-wide MR analyses to evaluate the causal effects of thousands of proteins across a wide range of disease outcomes[5,12–17], including osteoporosis-related traits[18–22]. However, earlier studies examined only a limited number of proteomics cohorts as exposure and limited outcomes[23–26]. Combining multiple proteomics cohorts with population-scale sample sizes and broad coverage[4,13,27,28], together with expanded fracture GWAS datasets[29], now make it possible to refine and extend earlier findings.

In this study, we applied proteome-wide MR to systematically estimate the causal effects of genetically determined circulating proteins on BMD and fracture risk. By combining the latest large-scale proteomic GWAS with GWAS of osteoporosis-related outcomes, we generated an updated and more comprehensive assessment of protein targets implicated in osteoporosis. We integrated evidence from two-sample MR, three Bayesian colocalization approaches, phenome-wide association studies (PheWAS), and druggability profiling to identify proteins with consistent genetic support as potential therapeutic targets for osteoporosis.

Materials and Methods

MR overview

We performed two-sample proteome-wide MR using circulating proteins as exposures and osteoporosis-related phenotypes as outcomes. For the protein GWAS, we used summary statistics from four of the largest single-cohort plasma-proteome GWAS currently available, each comprising individuals of European ancestry (described below). Summary statistics for osteoporosis outcomes were obtained from five independent BMD and fracture GWAS. All analyses adhered to the STROBE-MR reporting guidelines[11].

Proteomic exposure data

Plasma protein GWAS were originally conducted in four independent cohorts of European ancestry: the Atherosclerosis Risk in Communities (ARIC) study (7,213 participants, 4,657 proteins measured with SomaScan v4)[27], the Fenland study (10,708 participants, 4,775 proteins measured with SomaScan v4)[28], the deCODE cohort (35,559 participants, 4,907 proteins measured with SomaScan v4)[13], and the UK Biobank Pharma Proteomics Project (UKBPPP; 34,557 participants from the European-ancestry discovery cohort, 2,923 proteins measured with Olink Explore 3072)[4]. These datasets were used to define instrumental variables for MR, as described below.

Osteoporosis outcome data

We assessed five outcomes derived from individuals of European ancestry. The three BMD outcomes were heel quantitative-ultrasound estimated BMD (eBMD; N = 426,824) by Morris et al[30], femoral neck BMD (FN BMD; N = 32,735) from Zheng et al[31], and lumbar spine BMD (LS BMD; N = 28,498) from Zheng et al[31]. The two fracture outcomes were any fractures in the UK Biobank (N = 426,795; cases = 53,184)[30] and forearm fractures across eight Northern European biobanks (N = 1,021,094; cases = 50,471)[29].

Instrument definition and identification

Instruments for the protein exposures were defined according to criteria established in our previous work[16,32]. We use protein quantitative trait loci (pQTLs), which were genetic variants that influence plasma protein abundance. To reduce risk horizontal pleiotropy, we restricted instruments to *cis*-acting pQTLs (*cis*-pQTLs) within 500 kb of the transcription start site (TSS) of the corresponding protein-coding gene and associated at $P < 5\times10^{-8}$ because they are more likely to directly influence the protein abundance[16,32]. *Cis*-pQTLs mapping to genes in the HLA region (MICA, MICB) and to CD74 were excluded because of the complex linkage disequilibrium (LD) structure and high pleiotropy in this region[33]. LD clumping ($r^2 < 0.001$, 1 Mb window) was performed separately in each cohort using 50,000 unrelated European participants from the UK Biobank (UKB 50K) as the LD reference. We retained variants with minor allele frequency (MAF) > 0.01.

To further reduce risk of horizontal pleiotropy, we applied an additional “strict V2G” filtering step, as described previously[16,32]. In each cohort, we first retained only variants that were associated in *cis* with a single protein-coding gene (“strict” *cis*-pQTLs). We then evaluated these variants

using the Open Targets Genetics variant-to-gene (V2G) scoring system, which integrates multiple lines of evidence to prioritize likely causal genes. A variant was retained only if it had the highest V2G score for its associated protein-coding gene. Variants that passed both criteria formed the final set of strict V2G *cis*-pQTL instruments were used in the MR analyses. This selection process ensures that each genetic instrument is strongly associated with a single protein-coding gene, thereby minimizing the risk of violating MR assumptions and strengthening the validity of any inferred causal associations with osteoporosis outcomes.

Two-sample MR

We conducted two-sample proteome-wide MR to estimate the causal effects of genetically predicted protein levels on osteoporosis-related outcomes using the TwoSampleMR package (v.0.5.6). For clarity, we hereafter refer to "genetically predicted protein levels" simply by the protein's name. Causal effects for proteins with a single instrument were estimated using the Wald ratio, and those with multiple instruments were estimated using inverse-variance weighted (IVW). Statistically significant protein-outcome associations were identified using a Bejamin-Hochberg false discovery rate (FDR) threshold of 0.5%. To assess weak instrumental bias, we calculated F-statistics for all instruments and ensured that all exceeded 10.

Sensitivity analyses

We conducted several sensitivity analyses to assess the robustness of the MR estimates.

1) Alternative MR estimators:

For each protein, we re-estimated causal effects using three pleiotropy-robust methods: weighted median, weighted mode, and MR-Egger.

2) Between-instrument heterogeneity:

Heterogeneity was assessed using Cochran's Q statistic ($P > 0.05$) and the corresponding I^2 (< 50%). We classified results as Pass when $I^2 < 0.50$ or Q-value > 0.05, Fail when $I^2 \geq 0.50$ and Q-value ≤ 0.05, and NA for single-instrument models.

3) Directional horizontal pleiotropy:

MR relies on the assumption of no horizontal pleiotropy, which requires that the instruments used for MR analyses act on the target outcome exclusively through the exposure of interest. We tested this assumption using the MR-Egger intercept test when three or more instruments were available. Associations with an intercept $P \geq 0.05$ were considered Pass, whereas those with an intercept $P < 0.05$ were considered Fail, and single-instrument models were classified as NA.

In summary, a protein-outcome association was considered to "pass all sensitivity checks" if it met all of the following criteria: (i) FDR < 0.005; (ii) heterogeneity Pass/NA; and (iii) pleiotropy Pass/NA.

Bayesian colocalization

To assess whether circulating proteins and osteoporosis outcomes share the same underlying causal variant(s), and to mitigate confounding by LD, we employed three colocalization methods: coloc v.6.0.0[34], PWCoCo v.1.0[31], and SharePro v.5.0.0[35]. These methods accommodate scenarios with either single or multiple causal variants. A posterior probability for

a shared causal variant (PPH4) > 0.8 in any method was considered evidence of colocalization. Protein-outcome associations that passed MR sensitivity analyses and demonstrated colocalization were classified as having causal support.

Identifying robust and biologically relevant proteins

We applied three additional filters to protein-outcome pairs that passed MR and colocalization:

1. Cross-cohort replication: We retained only associations that passed MR and sensitivity analyses and demonstrated colocalization (PPH4 > 0.8) in at least two of the four cohorts.
2. Direction concordance: Among replicated associations, we required that their effect estimates were directionally concordant across the cohorts (i.e., β-coefficients showed the same sign).
3. Evidence of biological activity in circulation: We performed a literature review to confirm that each remaining protein has documented biological activity in plasma.

Phenome-wide association study of *TIMP2* and lead *cis*-pQTLs

We queried traits associated with *TIMP2* and the lead *cis*-pQTLs of *TIMP2* (rs11077399, rs9894212, rs931227, rs8066695) using the Association to Function (A2F) Knowledge Portal (https://a2f.hugeamp.org:8000/gene.html?gene=TIMP2). A2F uses GWAS summary statistics to calculate gene-level association scores with MAGMA (Multi-marker Analysis of GenoMic Annotation)[36]. For each trait, MAGMA aggregates all common variants within ±50 kb of a gene, adjusts their joint effects for LD using ancestry-matched 1000 Genomes reference panels, and reports a single *P* value per gene for each ancestry and at the trans-ethnic level. Gene-level associations reaching $P \leq 2.5 \times 10^{-6}$ are considered significant.

For variant-level PheWAS, A2F provides trait effect estimates (betas) with respect to each trait GWAS's effect allele. When this allele differed from the allele used in our harmonized data, we re-oriented the outcome to match the effect allele of lead *cis*-pQTLs of TIMP2 such that the A2F effect allele to ensure consistency in effect direction.

TIMP2 rare variant collapsing analysis

We obtained *TIMP2* rare variant collapsing results from the AstraZeneca UK Biobank program in individuals of European ancestry using the ptvraredmg model, which aggregates rare protein-truncating and predicted damaging missense variants into a qualifying variant (QV) carrier indicator. For each phenotype, we extracted the reported effect size (β in standard deviation [SD] units comparing QV carriers with non-carriers), standard error, 95% confidence interval (CI), two-sided *P*value, sample size, and counts of QV carriers and non-carriers. Primary outcomes were prespecified BMD T-score endpoints with direct clinical interpretation: heel BMD T-score, lumbar spine (L1-L4) T-score, femoral neck T-score (left), femur wards T-score (left), and femur total T-score (left). Secondary outcomes were the corresponding non-T-score BMD measures at the same skeletal sites, including heel eBMD and DXA-derived BMD at L1-L4, femoral neck, and femur total. When bilateral measures were available, we prioritized left-sided values to reduce redundancy. Reported associations were summarized without re-estimation of effect sizes and visualized using forest plots showing β and 95% CIs. *P* values were nominal,

and emphasis was placed on the directional concordance of effects across skeletal sites and imaging modalities.

Druggability assessment

For the prioritized 18 proteins, we calculated the average Z score of MR estimates across cohorts, capping values at ±10. Heatmaps were generated using pheatmap (R v4.1.2), with row annotations indicating druggability tiers (Tier 1-3) from Finan et al.[37] and the presence of each protein in the Open Targets and Drug Bank databases (Yes/No).

Results

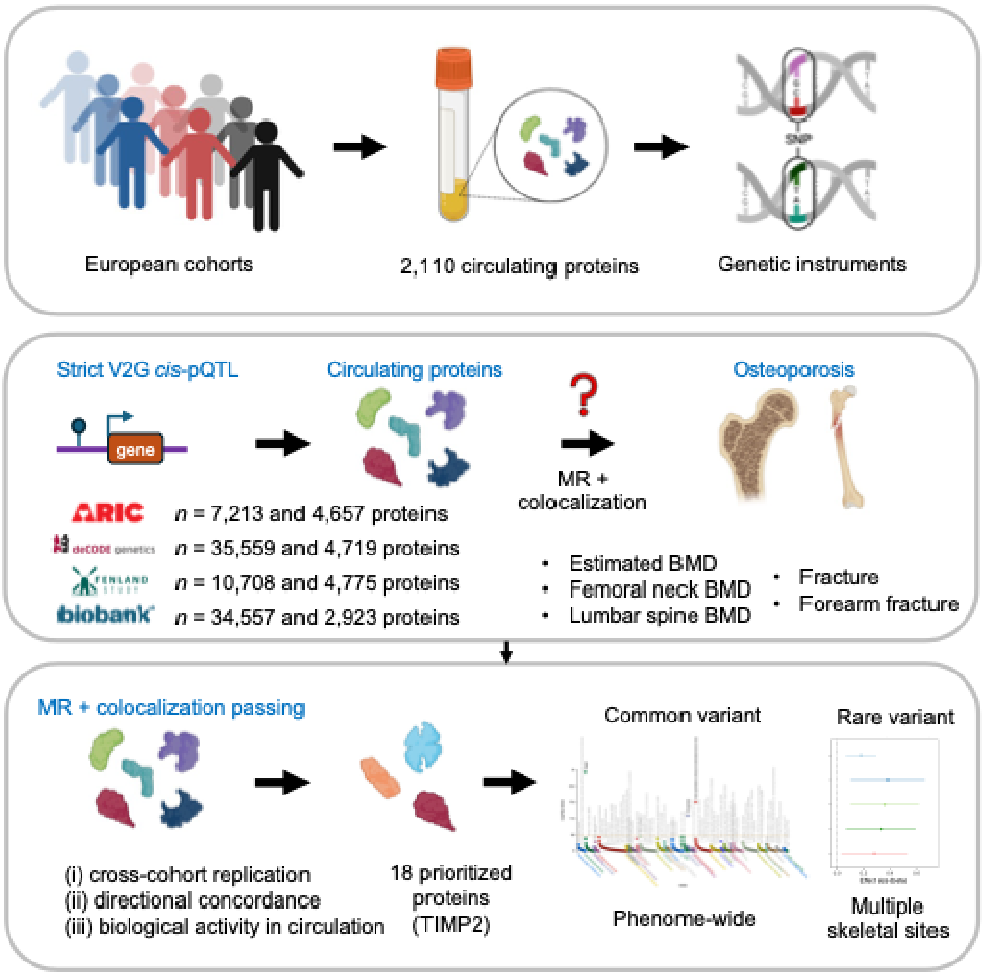
European cohorts
2,110 circulating proteins
Genetic instruments
Strict V2G cis-pQTL
Circulating proteins
Osteoporosis
gene
MR + colocalization
ARIC n = 7,213 and 4,657 proteins
deCODE genetics n = 35,559 and 4,719 proteins
FENLAND STUDY n = 10,708 and 4,775 proteins
biobank n = 34,557 and 2,923 proteins
Estimated BMD
Femoral neck BMD
Lumbar spine BMD
Fracture
Forearm fracture
MR + colocalization passing
(i) cross-cohort replication
(ii) directional concordance
(iii) biological activity in circulation
18 prioritized proteins (TIMP2)
Common variant
Rare variant
Phenome-wide
Multiple skeletal sites

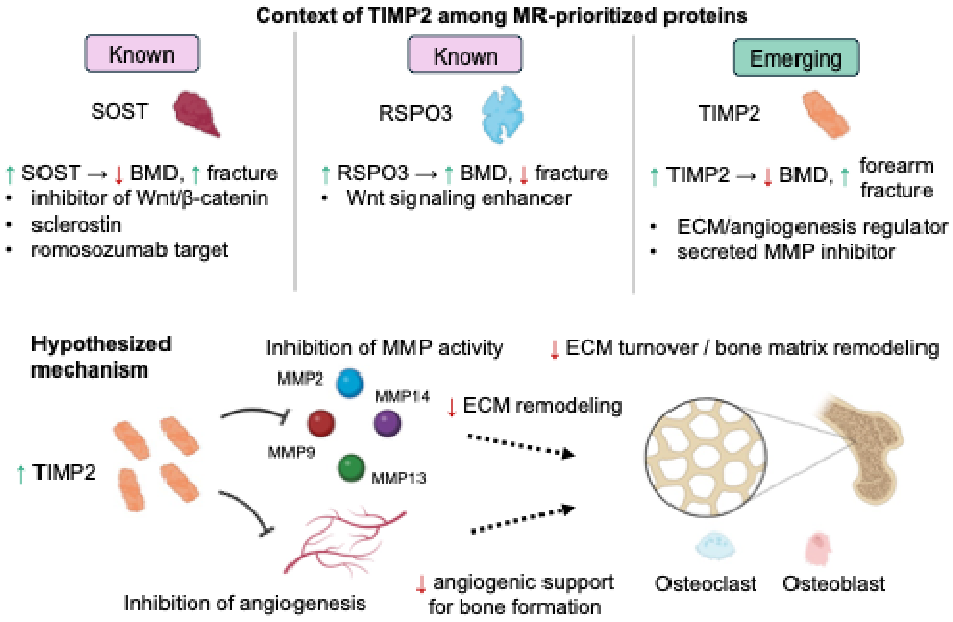
Context of TIMP2 among MR-prioritized proteins
Known
SOST
↑ SOST → ↓ BMD, ↑ fracture
inhibitor of Wnt/β-catenin
sclerostin
romosozumab target
Known
RSPO3
↑ RSPO3 → ↑ BMD, ↓ fracture
Wnt signaling enhancer
Emerging
TIMP2
↑ TIMP2 → ↓ BMD, ↑ forearm fracture
ECM/angiogenesis regulator
secreted MMP inhibitor
Hypothesized mechanism
Inhibition of MMP activity
↓ ECM turnover / bone matrix remodeling
MMP2
MMP14
MMP9
MMP13
↓ ECM remodeling
↑ TIMP2
Inhibition of angiogenesis
↓ angiogenic support for bone formation
Osteoclast
Osteoblast

Figure 1. Overview of study design and prioritization of TIMP2 as a therapeutic target for osteoporosis.

A) Genetic instrument selection. Proteomic and genetic data from four European-ancestry cohorts (ARIC, deCODE, Fenland, UKB-PPP) were aggregated, and *cis*-pQTLs were curated for 2,110 circulating proteins. Strict variant-to-gene (V2G) filtering was applied to retain genome-wide significant variants that map uniquely to a single protein-coding gene and have the strongest variant-to-gene evidence, yielding 6,224 independent *cis*-pQTL instruments.

B) Proteome-wide Mendelian randomization (MR), colocalization, and protein prioritization. Strict V2G *cis*-pQTLs were used as instruments in two-sample MR to estimate the causal effects of circulating proteins on five osteoporosis-related outcomes: heel estimated bone mineral density (BMD), femoral neck BMD, lumbar spine BMD, any fracture, and forearm fracture. Associations passing multiple-testing correction and MR sensitivity analyses were taken forward to Bayesian colocalization (coloc, PWCoCo, SharePro) to assess whether protein and outcome signals shared a causal variant. High-confidence proteins were then prioritized using three criteria: (i) cross-cohort replication, (ii) directional concordance of effect estimates, and (iii) evidence of biological activity in circulation, resulting in 18 MR- and colocalization-supported proteins, including TIMP2 (tissue inhibitor of metalloproteinases 2). TIMP2 was further characterized using common-variant phenome-wide association analyses and rare-variant collapsing analyses of bone traits across multiple skeletal sites.

C) Context of TIMP2 among MR-prioritized proteins. Among the 18 prioritized proteins, SOST and RSPO3 acted as internal biological benchmarks with well-established opposing effects on bone (SOST: higher protein levels associated with lower BMD and higher fracture risk; RSPO3: higher protein levels associated with higher BMD and lower fracture risk). TIMP2 emerged as a novel candidate, with higher genetically predicted circulating TIMP2 associated with lower BMD and increased forearm fracture risk, whereas rare damaging or loss-of-function TIMP2 variants were associated with higher BMD.

D) Proposed mechanism for TIMP2 in bone remodelling. TIMP2 is a secreted inhibitor of matrix metalloproteinases (including MMP14, MMP2, and MMP13) that regulate extracellular matrix (ECM) turnover and angiogenesis. Elevated TIMP2 is hypothesized to reduce MMP activity, leading to impaired ECM remodelling, altered osteoclast–osteoblast coupling, and reduced angiogenic support for bone formation, thereby lowering BMD. Conversely, genetic reductions in TIMP2 activity are associated with increased BMD.

Study overview

The study design is shown in **Figure 1**.

Genetic instrument selection

The genetic instrument selection process is shown in **Supplementary Figure 1**. We curated *cis*-pQTLs from four European ancestry cohorts[4,13,27,28] (**Supplementary Table 1**). In total, 6,224 independent *cis*-pQTLs instrumenting 2,110 circulating proteins (1,106 in ARIC, 1,247 in deCODE, 1,198 in Fenland, 1,294 in UKBPPP) remained after LD clumping and our strict V2G criteria. Briefly, strict V2G *cis*-pQTLs are genome-wide significant variants associated with a

single protein-coding gene and showing the strongest variant-to-gene support according to the Open Targets Genetics V2G score. There was no evidence of weak instrument bias (median F-statistics = 255, 298, 233, 448 across ARIC, deCODE, Fenland, and UKB-PPP cohorts, respectively; range 30–13,425). (**Supplementary Table 2**).

Two-sample proteome-wide MR

We estimated the causal effects of circulating proteins on osteoporosis-related traits using two-sample MR. Strict V2G *cis*-pQTLs served as instrumental variables, and the five outcomes were eBMD, FN BMD, LS BMD, any fracture, and forearm fracture (**Supplementary Table 1**). For each cohort, harmonized protein-outcome summary statistics used for MR are provided in **Supplementary Tables 3-6**, respectively. Using a Benjamini Hochberg-corrected FDR threshold of 0.5% in each outcome for each cohort, we identified 192 unique protein-outcome associations (180 for eBMD; 2 for FN BMD; 2 for LS BMD; 2 for fracture; 6 for forearm fracture) that met MR and sensitivity analysis criteria, including heterogeneity and directional horizontal pleiotropy (**Supplementary Table 7**).

Bayesian colocalization and prioritization of high-confidence proteins

To reduce the possibility that MR results were not biased by LD, we conducted Bayesian colocalization using three methods (coloc, PWCoCo and SharePro). A posterior probability for a shared causal variant (PPH4 > 0.8) in any method was obtained for 128 protein-outcome pairs (117 for eBMD; 2 for FN BMD; 1 for LS BMD; 2 for fracture; 6 for forearm fracture), representing 67% of MR-significant associations (**Supplementary Table 8**).

To identify robust and biologically relevant proteins, we applied three criteria: (i) cross-cohort replication, (ii) directional concordance, and (iii) documented biological activity in circulation. Forty-six protein-outcome associations involving 42 proteins replicated across cohorts with concordant effect directions (**Supplementary Table 9**). Of these, 22 associations (8%) spanning 18 proteins had evidence of biological activity in circulation: ANGPTL4, C5, CTSS, EGF, FRZB, GDF15, ITIH3, KNG1, OLFML3, PLAU, PLTP, RSPO3, SERPINF2, SERPING1, SMOC2, SOST, TIMP2, and TGFBI (**Supplementary Table 10**). The corresponding 22 associations are provided in **Supplementary Table 11**.

Two well-established skeletal regulators, SOST (sclerostin) and RSPO3 (R-spondin-3), served as internal validation markers. As expected from their known biological roles[38–40], the two proteins showed strong but opposing associations with BMD and fracture risk. SOST, which suppresses osteoblast activity, was negatively associated with eBMD (β_{UKBPPP} = -0.51, P_{UKBPPP} = 6.1 × 10^{-59}; **Figure 2**) and FN BMD ($\beta_{Fenland}$ = -0.59, $P_{Fenland}$ = 9.4 × 10^{-8}; **Figure 3a**), and was positively associated with both overall fracture risk ($\beta_{Fenland}$ = 0.096, $P_{Fenland}$ = 2.7 × 10^{-12}; **Figure 3b**) and forearm fracture risk ($\beta_{Fenland}$ = 0.10, $P_{Fenland}$ = 6.9 × 10^{-25}; **Figure 3b**). RSPO3, a stimulator of osteoblast differentiation via Wnt signaling, showed positive associations with eBMD ($\beta_{Fenland}$ = 0.21, $P_{Fenland}$ < 2.3 × 10^{-308}; **Figure 2**) and was negatively associated with both overall fracture risk ($\beta_{Fenland}$ = -0.18, $P_{Fenland}$ = 8.3 × 10^{-21}; **Figure 3b**) and forearm fracture risk (β_{ARIC} = -0.22, P_{ARIC} = 9.1 × 10^{-51}; **Figure 3b**). For each protein, we report the association with the lowest *P* value observed across cohorts.

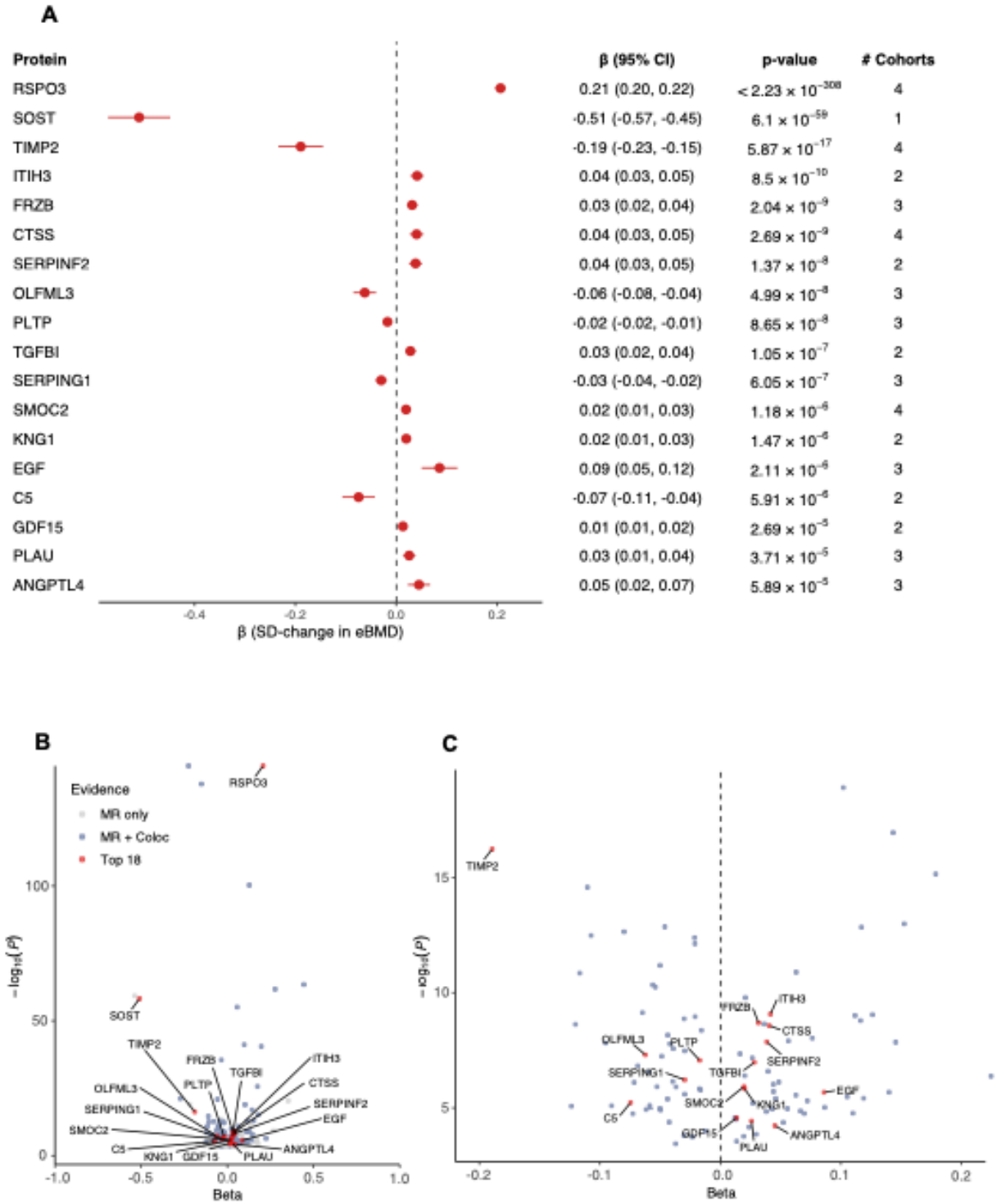

Figure 2. Proteome-wide Mendelian randomization associations of circulating proteins with heel estimated BMD (eBMD).

(A) Forest plot of the 18 MR- and colocalization-prioritized proteins with evidence of biological activity in circulation. For each protein, the point denotes the MR effect estimate (β, SD change in eBMD per 1 SD higher genetically predicted protein level) from the cohort with the smallest *P*

value, and the horizontal bar shows the 95% confidence interval (CI). The accompanying table reports β (95% CI), *P* value, and the number of proteomic cohorts in which the protein-eBMD association passed MR and colocalization criteria. Positive β values indicate higher eBMD and negative β values indicate lower eBMD; SOST and TIMP2 show the largest negative effects, whereas RSPO3 shows a strong positive effect.

(B) Volcano plot of all proteins showing MR associations with eBMD at FDR ≤ 0.5% across the four proteomic cohorts. The *x*-axis shows the MR effect estimate (β) and the y-axis shows -$\log_{10}(P)$. Points are colored by level of evidence: proteins passing MR only (grey), proteins passing both MR and colocalization (blue), and the 18 prioritized proteins shown in panel A (red), with selected proteins labelled.

(C) Zoomed view of the volcano plot in panel B, highlighting the position of the 18 prioritized proteins, including TIMP2, SOST, and RSPO3.

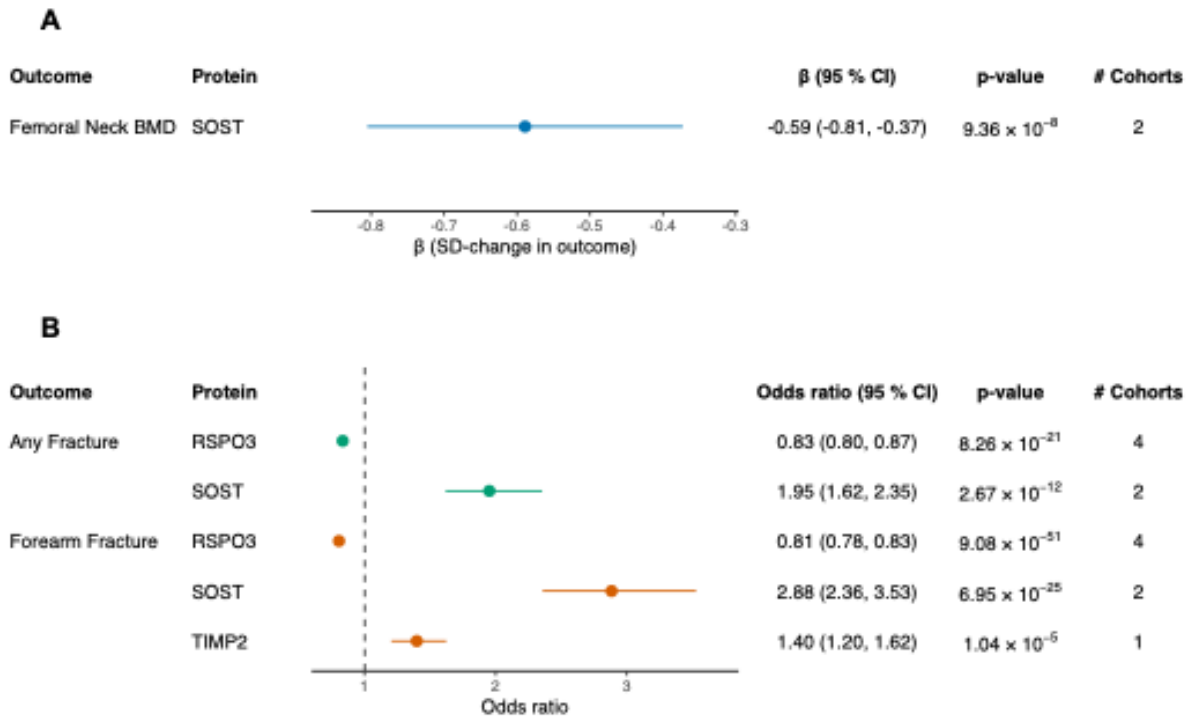

Figure 3. Mendelian randomization (MR) estimates of SOST, RSPO3, and TIMP2 on femoral neck bone mineral density (BMD) and fracture risk.

(A) Forest plot showing the association between genetically predicted circulating SOST and femoral neck BMD (SD units). The point represents the MR effect estimate (β) and the horizontal bar indicates the 95% confidence interval (CI) from the cohort with the smallest *P* value (Fenland); the table indicates β (95% CI), *P* value, and the number of proteomic cohorts in which the SOST-femoral neck BMD association passed MR and colocalization criteria.

(B) Forest plot showing MR-derived odds ratios (ORs) for any fracture and forearm fracture per 1 SD higher genetically predicted protein level for RSPO3, SOST, and TIMP2. Points represent ORs and horizontal bars show 95% CIs, with the vertical dashed line denoting the null (OR = 1).

For each protein-outcome pair, the estimate from the cohort with the smallest *P* value is displayed, together with its OR, 95% CI, *P* value, and the number of cohorts in which the association replicated. RSPO3 shows protective associations with fracture risk, whereas SOST and TIMP2 show increased fracture risk, consistent with their directions of effect on BMD.

Among the less characterized proteins, TIMP2 (tissue inhibitor of metalloproteinases 2) emerged as a compelling target. TIMP2 is a secreted inhibitor of matrix metalloproteinases (MMPs) that regulates extracellular matrix turnover and independently suppresses endothelial-cell proliferation, making it an important modulator of tissue remodelling in both health and disease. At an FDR threshold of 0.5%, a one SD increase in genetically predicted circulating TIMP2 was associated with lower eBMD in all four proteomic cohorts (β_{ARIC} = -0.085, β_{deCODE} = -0.19, $\beta_{Fenland}$ = -0.15, β_{UKBPPP} = -0.14, $P_{ARIC} = 1.08 \times 10^{-7}$, $P_{deCODE} = 5.9 \times 10^{-17}$, $P_{Fenland} = 1.4 \times 10^{-9}$, $P_{UKBPPP} = 1.1 \times 10^{-12}$; **Figure 2**), with consistent direction and broadly similar effect sizes across cohorts. These associations were supported by strong colocalization evidence ($PPH4_{ARIC}$ = 1.00, $PPH4_{deCODE}$ = 1.00, $PPH4_{Fenland}$ = 0.913, $PPH4_{UKBPPP}$ = 1.00). Additionally, a one SD increase in genetically predicted TIMP2 levels was associated with a higher risk of forearm fracture in the UKBPPP cohort (β_{UKBPPP} = 0.34, $P_{UKBPPP} = 1.04 \times 10^{-5}$, $PPH4_{UKBPPP}$ = 0.90; **Figure 3b**), consistent with the direction of the eBMD findings. The lead *cis*-pQTL for TIMP2 differed across cohorts, consistent with differences in proteomic measurement platforms (Somascan vs. Olink) and underlying population genetic architecture: rs11077399 in ARIC, rs9894212 in deCODE, rs931227 in Fenland, and rs8066695 in UKBPPP.

Phenome-wide association analyses for *TIMP2*

To obtain orthogonal evidence, we examined *TIMP2* gene- and variant-level associations in the A2F Knowledge Portal, which reports MAGMA-based gene-level scores. Common variants at *TIMP2* showed significant gene-level associations with eBMD ($P = 2.96 \times 10^{-18}$), height ($P = 6.34 \times 10^{-29}$), and phosphate levels ($P = 1.76 \times 10^{-13}$), all musculoskeletal traits (**Figure 4** and **Supplementary Table 12**).

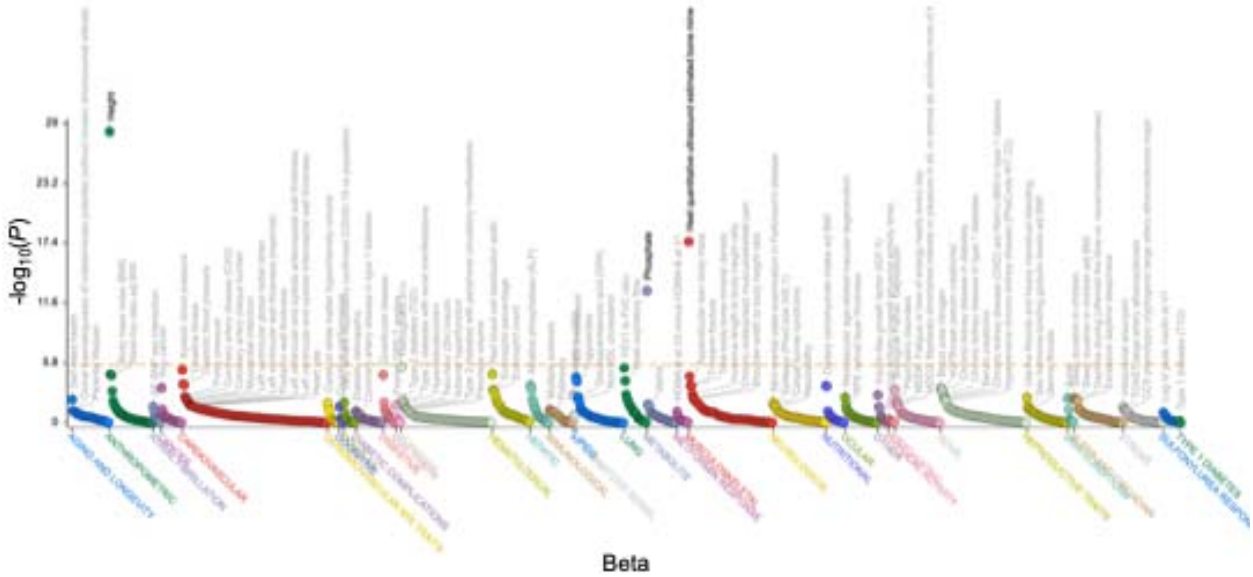

Figure 4. Phenome-wide association results for *TIMP2* based on common-variant gene-based associations from mixed-ancestry gene-level analyses in the Association-to-Function (A2F) Knowledge Portal.
Each point represents the MAGMA gene-level association between *TIMP2* and a complex trait, plotted by the effect estimate (β; x-axis) and $-\log_{10}(P)$ (y-axis). Traits are grouped by phenotype category, with distinguished by color. The horizontal orange dashed line indicates the significance threshold used by A2F ($P \leq 2.5 \times 10^{-6}$).

We next examined variant-level associations for each cohort's lead *cis*-pQTL (ARIC: rs11077399; deCODE: rs9894212; Fenland: rs931227; UKBPPP: rs8066695). Across cohorts, alleles that increased circulating TIMP2 were consistently associated with lower eBMD, whereas TIMP2-decreasing alleles were associated with higher eBMD, mirroring the MR directionality (**Supplementary Figure 2-5**). When effects were aligned to the TIMP2-increasing allele for rs11077399, rs931227, and rs8066695, these variants showed inverse associations with eBMD (rs11077399: $\beta = -0.012$, $P = 4.4 \times 10^{-9}$; rs931227: $\beta = -0.015$, $P = 9.5 \times 10^{-12}$; rs8066695: $\beta = -0.014$, $P = 7.6 \times 10^{-13}$) and height (rs11077399: $\beta = -0.010$, $P = 3.9 \times 10^{-25}$; rs931227: $\beta = -0.011$, $P = 2.1 \times 10^{-15}$; rs8066695: $\beta = -0.010$, $P = 3.6 \times 10^{-32}$). The effect allele of rs931227 was positively associated with body mass index ($\beta = 0.011$, $P = 2.0 \times 10^{-9}$), while the effect allele of rs8066695 was negatively associated with phosphate levels ($\beta = -0.016$, $P = 1.2 \times 10^{-14}$). In contrast, the TIMP2-decreasing allele at rs9894212 was associated with higher eBMD ($\beta = 0.016$, $P = 1.65 \times 10^{-12}$) and greater height ($\beta = -0.006$, $P = 7.75 \times 10^{-10}$), consistent with our MR results. Full per-variant PheWAS results are provided in **Supplementary Table 13-16**.

Taken together, gene- and variant-level PheWAS converged on bone-related associations with little evidence of non-skeletal pleiotropy, supporting TIMP2 as a promising therapeutic target for osteoporosis.

TIMP2 rare variant collapsing analysis on T-score and non-T-score BMD measures in the UK Biobank

In the AstraZeneca UK Biobank gene-level collapsing analysis of European ancestry participants, carriers of rare, predicted damaging or loss-of-function (LoF) variants in *TIMP2* had higher BMD T-scores across multiple skeletal sites (**Supplementary Table 17** and **Figure 5a**). Heel BMD T-score was higher in carriers (β = 0.180, 95% CI: 0.066 to 0.294; $P = 2.0 \times 10^{-3}$; N = 262,441; QV = 273). Lumbar spine (L1-L4) T-score was also higher (β = 0.39, 95% CI: 0.099 to 0.68; $P = 8.6 \times 10^{-3}$; N = 42,991; QV = 42). At the left hip, femoral neck T-score (β = 0.40, 95% CI: 0.12 to 0.68; $P = 4.9 \times 10^{-3}$; N = 45,187; QV = 46), femur wards T-score (β = 0.34, 95% CI: 0.067 to 0.62; P = 0.015; N = 45,183; QV = 46), and femur total T-score (β = 0.30, 95% CI: 0.019 to 0.57; P = 0.036; N = 45,120; QV = 46) were all higher in carriers than in non-carriers. Corresponding non-T-score BMD measures at the same sites showed the same positive direction of effect with slightly attenuated estimates (**Supplementary Table 17** and **Figure 5b**), indicating a consistent but modest protective effect of rare, predicted damaging *TIMP2* variants on BMD across measurement modalities.

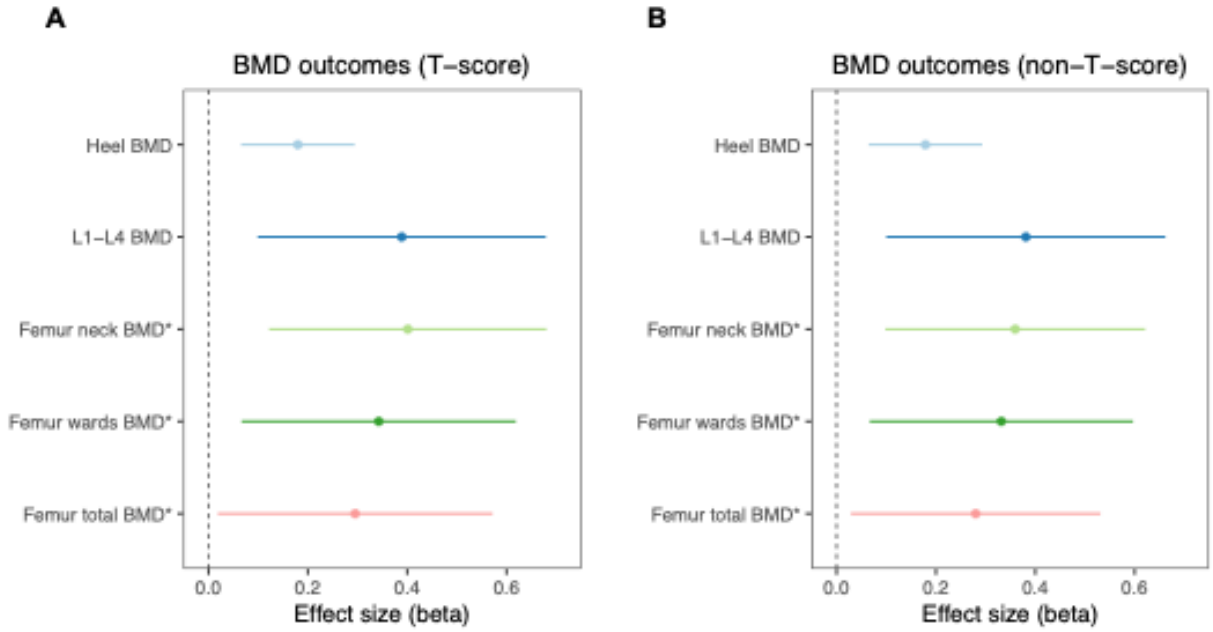

Figure 5. Associations between rare damaging or loss-of-function (LoF) *TIMP2* variants and bone mineral density (BMD) outcomes.

Panels A and B show forest plots of the associations between carriage of qualifying rare variants in *TIMP2* (ptvraredmg collapsing model) and BMD outcomes in European-ancestry individuals: panel A presents the five prespecified T-score endpoints (heel BMD, lumbar spine L1-L4, femoral neck, femur wards, and femur total), and panel B presents the corresponding non-T-score BMD measures at the same skeletal sites. Points indicate regression coefficients (β) and horizontal lines show 95% confidence intervals, with positive β values indicating higher BMD among carriers of a qualifying variant compared with non-carriers. *Left-sided skeletal endpoints are shown.

Druggability assessment of MR-prioritized proteins

We assessed druggability of the 18 MR- and colocalization-prioritized proteins using three complementary resources: the druggable genome classification (Tiers 1–3), DrugBank, and the Open Targets Platform. The druggable genome framework stratifies proteins by druggability potential, DrugBank catalogs approved and investigational drugs and their targets, and Open Targets links targets to diseases and clinical development stages.

All 18 proteins mapped to the druggable genome, with three proteins (SOST, C5, CTSS) in Tier 1 and one (PLAU) in Tier 2 (**Figure 6**). Half of the 18 proteins had approved or investigational drugs in DrugBank, and four were listed as targets in the Open Targets Platform (**Figure 6**). Notably, TIMP2 was a Tier 3 secreted protein that did not appear in Drug Bank or Open Targets, indicating a lack of prior therapeutic targeting but suggesting therapeutic potential given its extracellular activity and strong genetic evidence for a causal role in bone.

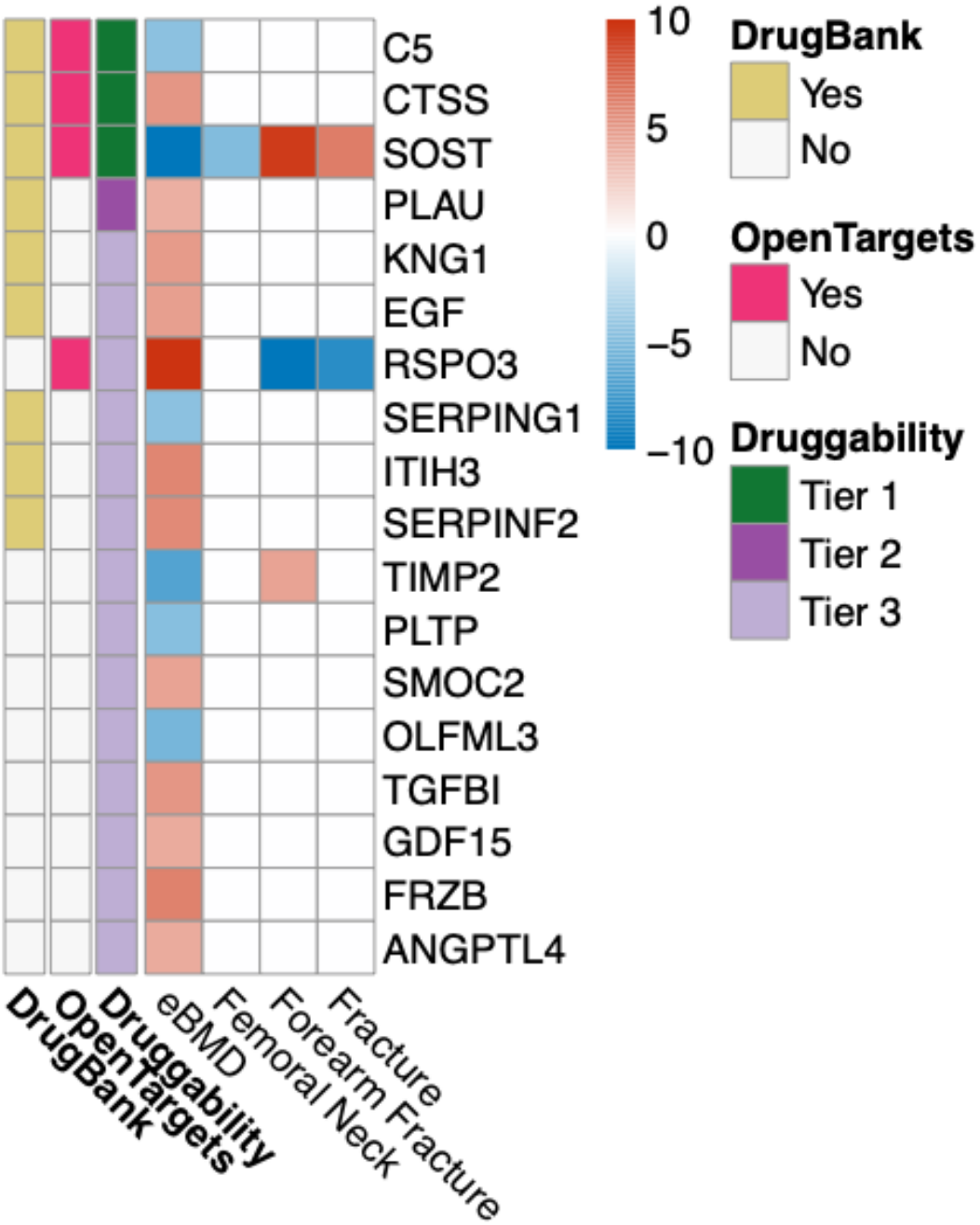

Figure 6. Mendelian randomization (MR) associations between circulating proteins and bone phenotypes with druggability annotations.

Heatmap showing Z-scores for the association between genetically predicted circulating levels of 18 MR-prioritized proteins and four outcomes: estimated bone mineral density (eBMD), femoral neck BMD, forearm fracture, and any fracture. Each cell represents the mean MR Z-score for a given protein-outcome pair across European-ancestry cohorts, truncated at ±10. Red and blue denote positive and negative Z-scores, respectively. Proteins (rows) are ordered by druggability tier from Finan et al. (Tier 1–3)[37] and, within tiers, by the amount of external drug

evidence. Row annotations indicate the Finan druggability tier and whether the corresponding target is listed in Open Targets or Drug Bank (Yes/No).

Discussion

In this study, we performed large-scale proteome-wide MR analyses and identified 18 circulating proteins with putative causal effects on BMD and fracture risk. These analyses recapitulated two established regulators of skeletal homeostasis, SOST and RSPO3, and also highlighted less characterized proteins, most notably TIMP2, as a compelling candidate. PheWAS further showed that genetically predicted TIMP2 levels are strongly associated with musculoskeletal traits and exhibit minimal associations with non-skeletal phenotypes, supporting a predominantly bone-specific role for TIMP2.

Consistent with these findings, our MR and gene-based collapsing analyses support an inhibitory role of TIMP2 in skeletal mineralization. Higher genetically predicted circulating TIMP2, reflecting reduced MMP activity, was associated with lower BMD, whereas rare LoF or predicted damaging TIMP2 variants were associated with higher BMD. Across heel, lumbar spine, and left hip, carriers of such variants exhibited higher BMD T-scores together with concordant increases in non-T-score BMD measures. These collapsing results were directionally concordant with the MR findings for eBMD and collectively support a model in which reduced TIMP2 activity promotes bone mineral accrual and increases BMD at clinically relevant skeletal sites. The concordance between primary T-score endpoints and secondary BMD measures, together with consistency across heel, spine, and hip, argues against a site-specific artifact and instead suggests a generalized skeletal effect of TIMP2 inhibition.

TIMP2 is a secreted inhibitor of MMPs, a family of zinc-dependent peptidases that mediate extracellular matrix (ECM) degradation[41]. MMP activity, particularly that of MMP2, MMP9, MMP13, and MMP14, modulates several key steps of bone remodelling[42]. In mice, targeted deletion of these MMPs that regulate bone remodelling leads to reduced bone mineralization and severe skeletal abnormalities[43–46], demonstrating that adequate MMP activity is required for normal skeletal development. Consistent with these experimental data, in humans biallelic loss-of-function variants in MMP2 cause hereditary skeletal disorders such as multicentric osteolysis with nodulosis and arthropathy (MONA), Torg, and Winchester syndromes[47–51]. TIMP2 is expressed by osteoblast-lineage cells[52] and regulates MMP-mediated ECM turnover and osteoclast activity in a dose- and context-dependent manner. At higher concentrations, TIMP2 acts as a broad MMP inhibitor with strong affinity for MMP-2, thereby suppressing bone resorption[53]. At lower concentrations, however, TIMP2 participates in the MMP14-dependent activation of pro-MMP2[54], which can enhance resorptive activity[55]. Since skeletal homeostasis requires a balanced MMP2/MMP14/TIMP2 axis, chronically elevated TIMP2 may uncouple bone formation and resorption by excessively inhibiting matrix turnover.

TIMP2 is also unique among TIMP family members in its ability to directly inhibit endothelial cell proliferation independently of MMP inhibition[56,57], suggesting that elevated TIMP2 could additionally impair angiogenic support for bone formation. Although dedicated TIMP2-knockout studies remain limited, TIMP2-deficient mice develop accelerated osteoarthritis driven by increased angiogenesis[58]. Consistent with this, the Mouse Genome Informatics database reports that *Timp2*-mutant mice exhibit reduced bone mineral content. TIMP2 expression also declines with age in osteoblasts and osteocytes in mouse long bones[59], suggesting that TIMP2

may contribute to the maintenance of skeletal integrity during aging. However, this observation is correlative and does not establish a causal role.

Our study provides the first causal genetic evidence that elevated circulating TIMP2 influences BMD and fracture risk. Taken together with existing experimental and observational data, these findings support a model in which increased systemic TIMP2 reduces BMD through systemic over-inhibition of MMP-mediated bone remodelling and potentially diminished angiogenic support for bone formation. Further mechanistic work is warranted to delineate how TIMP2 regulates skeletal homeostasis.

In addition to TIMP2, our study re-identified known skeletal regulators SOST and RSPO3, which served as internal positive controls. SOST encodes sclerostin, an osteocyte-derived secreted glycoprotein that negatively regulates bone formation by inhibiting Wnt/β-catenin signalling and thereby suppressing osteoblast differentiation and activity[39,40]. Sclerostin is the target of the approved anabolic therapy romosozumab used to treat severe post-menopausal osteoporosis. Sclerostin's known role is consistent with our findings, which show its negative association with BMD and increased fracture risk. Conversely, RSPO3 encodes R-spondin-3, a secreted ligand that stimulates osteoblast activity and promotes bone formation by acting as an enhancer of Wnt signalling[38]. As expected, it showed a positive association with BMD and decreased fracture risk.

Among the other replicated proteins, CTSS (cathepsin S) and SMOC2 (SPARC related modular calcium binding 2) showed consistent positive associations with BMD across all four cohorts. CTSS is a secreted cysteine protease that has previously been implicated in bone remodeling[60]. Although CTSS and C5 (complement component 5) scored highly in druggability assessments, their broad immunological roles and extensive pleiotropy make them less attractive therapeutic targets for osteoporosis[60,61]. SMOC2 is a matricellular protein whose deficiency in mice has been linked to impaired periodontal bone healing and age-related skeletal deterioration, consistent with its positive association with BMD[62].

Several additional proteins not previously implicated in bone biology, including ITIH3, PLTP, SERPINF2, SERPING1, and OLFML3, also showed consistent causal associations with BMD in our analyses. These findings raise the possibility that they represent novel, uncharacterized regulators of skeletal homeostasis and warrant further functional investigation.

This study has several strengths. First, we integrated data from more than 100,000 individuals across four proteomics cohorts measured on complementary platforms (SomaScan and Olink), enabling both cross-cohort and cross-platform validation. TIMP2 showed a consistent association with reduced eBMD in all four cohorts, providing strong support for a causal role in BMD regulation. Second, we also extended previous proteome-wide MR studies of osteoporosis by evaluating a broader set of clinically relevant outcomes, including multiple site-specific BMD measures (eBMD, FN BMD, LS BMD) and both general and forearm fracture. Third, we implemented stringent "strict V2G" filtering to select genetic instruments, ensuring that each *cis*-pQTL was strongly and uniquely mapped to a single protein-coding gene and thereby reducing

the risk of horizontal pleiotropy. Finally, we applied three state-of-the-art colocalization methods that account for both single and multiple causal variants, mitigating confounding by LD and increasing confidence in the MR results.

This study also has some limitations. First, our MR and colocalization analyses were restricted to individuals of European ancestry. Osteoporosis-related GWAS are still predominantly derived from individuals of European ancestry, and available non-European datasets remain relatively small and underpowered, limiting their suitability for MR. Second, we could not perform sex-stratified analyses because sex-specific proteomic and outcome summary statistics were unavailable, even though sex differences in osteoporosis risk are well-established[1]. Third, fracture GWAS remain less powered than BMD GWAS, which may have contributed to the smaller number of fracture associations detected. Lastly, our work is limited to genetic analyses and does not include functional validation. Follow-up experimental studies and, ultimately, clinical trials will be necessary to confirm the therapeutic potential of targeting TIMP2.

In conclusion, by integrating proteome-wide MR with rigorous sensitivity analyses, colocalization, PheWAS, and rare-variant collapsing analyses, we identified 18 proteins with evidence for causal effects on BMD and osteoporosis risk, including the established regulators SOST and RSPO3 and the emerging candidate TIMP2. Our findings highlight TIMP2 as a biologically supported, bone-specific therapeutic target and emphasize the need for further functional and translational studies to clarify its role in skeletal metabolism.

Acknowledgements

C.-Y.S. is supported by a CIHR Canada Graduate Scholarship Doctoral Award (Funding Reference Number: 187673), an FRQS doctoral training scholarship, and a Lady Davis Institute/TD-Bank Scholarship. M.H. is supported by a Graduate Scholarship for Degree-Seeking Study Abroad from the Japan Student Services Organization (JASSO) under the special priority framework for doctoral studies at top-tier global universities in STEM fields, and by the 6th Toshizo Watanabe International Scholarship from The Watanabe Foundation. The funders had no role in the study design, data collection and analysis, decision to publish, or preparation of the manuscript. The Yoshiji Lab is supported by the Canada Research Chairs Program (CRC-2025-00097), the Canadian Institutes of Health Research (183596), the DNA to RNA (D2R) Foundational Program, Japan Society for the Promotion of Science, and McGill University.

Funding

There was no direct funding for performing this study.

Author contributions

Chen-Yang Su: Conceptualization; data curation; formal analysis; methodology; software; validation; visualization; writing – original draft; writing – review and editing.

Maya Akerman: Formal analysis; visualization; writing – original draft; writing – review and editing.

Masashi Hasebe: Writing – review and editing.

Satoshi Yoshiji: Conceptualization; writing – review and editing; supervision.

Conflict of Interest

SY serves as a consultant to the Broad Institute of MIT and Harvard through Precision Global Consulting and to PriveBio, Inc., unrelated to this project. All other authors report no conflicts of interest.

Data Availability

MR results can be accessed in the Supplementary Tables. All MR analyses adhered to STROBE-MR guidelines[11] (**Supplementary Note 1**).

References

1. Xiao, P.-L. *et al.* Global, regional prevalence, and risk factors of osteoporosis according to the World Health Organization diagnostic criteria: a systematic review and meta-analysis. *Osteoporos Int* **33**, 2137–2153 (2022).
2. Johnell, O. & Kanis, J. A. An estimate of the worldwide prevalence and disability associated with osteoporotic fractures. *Osteoporos Int* **17**, 1726–1733 (2006).
3. Reid, I. R. & Billington, E. O. Drug therapy for osteoporosis in older adults. *The Lancet* **399**, 1080–1092 (2022).
4. Sun, B. B. *et al.* Plasma proteomic associations with genetics and health in the UK Biobank. *Nature* **622**, 329–338 (2023).
5. Emilsson, V. *et al.* Co-regulatory networks of human serum proteins link genetics to disease. *Science* **361**, 769–773 (2018).
6. Lehallier, B. *et al.* Undulating changes in human plasma proteome profiles across the lifespan. *Nat Med* **25**, 1843–1850 (2019).
7. Schini, M., Vilaca, T., Gossiel, F., Salam, S. & Eastell, R. Bone Turnover Markers: Basic Biology to Clinical Applications. *Endocr Rev* **44**, 417–473 (2023).
8. Johansson, H. *et al.* A Meta-Analysis of Reference Markers of Bone Turnover for Prediction of Fracture. *Calcif Tissue Int* **94**, 560–567 (2014).
9. Su, C.-Y. *et al.* Circulating proteins to predict COVID-19 severity. *Sci Rep* **13**, 6236 (2023).
10. Carrasco-Zanini, J. *et al.* Proteomic signatures improve risk prediction for common and rare diseases. *Nat Med* **30**, 2489–2498 (2024).
11. Skrivankova, V. W. *et al.* Strengthening the reporting of observational studies in epidemiology using mendelian randomisation (STROBE-MR): explanation and elaboration. *BMJ* **375**, n2233 (2021).
12. Sun, B. B. *et al.* Genomic atlas of the human plasma proteome. *Nature* **558**, 73–79 (2018).
13. Ferkingstad, E. *et al.* Large-scale integration of the plasma proteome with genetics and disease. *Nat Genet* **53**, 1712–1721 (2021).
14. Zheng, J. *et al.* Phenome-wide Mendelian randomization mapping the influence of the plasma proteome on complex diseases. *Nat Genet* **52**, 1122–1131 (2020).
15. Yoshiji, S. *et al.* Proteome-wide Mendelian randomization implicates nephronectin as an actionable mediator of the effect of obesity on COVID-19 severity. *Nat Metab* **5**, 248–264 (2023).
16. Su, C.-Y. *et al.* Multi-ancestry proteome-phenome-wide Mendelian randomization offers a comprehensive protein-disease atlas and potential therapeutic targets. 2024.10.17.24315553 Preprint at https://doi.org/10.1101/2024.10.17.24315553 (2024).
17. Yoshiji, S. *et al.* Integrative proteogenomic analysis identifies COL6A3-derived endotrophin as a mediator of the effect of obesity on coronary artery disease. *Nat Genet* 1–13 (2025) doi:10.1038/s41588-024-02052-7.
18. Wang, H., Zhou, W., Huang, Y., Li, Y. & Zhang, K. Causal effects and mediation pathways of circulating plasma proteins on osteoporosis: a two-sample and two-step Mendelian randomization study. *Clinical Proteomics* **22**, 38 (2025).
19. Wang, L. *et al.* Assessing the causal relationship between plasma proteins and osteoporosis: novel insights into pathological mechanisms and therapeutic implications. *Osteoporos Int* **35**, 1973–1987 (2024).

20. Zheng, Y. *et al.* Plasma proteomic profiles reveal proteins and three characteristic patterns associated with osteoporosis: A prospective cohort study. *Journal of Advanced Research* **75**, 491–503 (2025).
21. Han, B.-X. *et al.* Causal Effects of Plasma Proteome on Osteoporosis and Osteoarthritis. *Calcif Tissue Int* **112**, 350–358 (2023).
22. Hasebe, M., Su, C.-Y., Kiel, D. P. & Yoshiji, S. Leveraging Proteomics and Proteogenomics for Understanding Osteoporosis and Other Musculoskeletal Diseases. *Curr Osteoporos Rep* **23**, 43 (2025).
23. Zheng, J. *et al.* Mendelian Randomization Analysis Reveals a Causal Influence of Circulating Sclerostin Levels on Bone Mineral Density and Fractures. *J Bone Miner Res* **34**, 1824–1836 (2019).
24. Keller-Baruch, J., Forgetta, V., Manousaki, D., Zhou, S. & Richards, J. B. Genetically Decreased Circulating Vascular Endothelial Growth Factor and Osteoporosis Outcomes: A Mendelian Randomization Study. *J Bone Miner Res* **35**, 649–656 (2020).
25. Yuan, S., Wan, Z.-H., Cheng, S.-L., Michaëlsson, K. & Larsson, S. C. Insulin-like Growth Factor-1, Bone Mineral Density, and Fracture: A Mendelian Randomization Study. *J Clin Endocrinol Metab* **106**, 1552–1558 (2021).
26. Cheng, T. *et al.* Genetic Evidence Supporting a Causal Association Between mTOR-Dependent EIF-4E Circulating Protein Level and Osteoporosis. *Adv Ther* **40**, 4987–4998 (2023).
27. Zhang, J. *et al.* Plasma proteome analyses in individuals of European and African ancestry identify cis-pQTLs and models for proteome-wide association studies. *Nat Genet* **54**, 593–602 (2022).
28. Pietzner, M. *et al.* Mapping the proteo-genomic convergence of human diseases. *Science* **374**, eabj1541 (2021).
29. Nethander, M. *et al.* An atlas of genetic determinants of forearm fracture. *Nat Genet* **55**, 1820–1830 (2023).
30. Morris, J. A. *et al.* An atlas of genetic influences on osteoporosis in humans and mice. *Nat Genet* **51**, 258–266 (2019).
31. Zheng, H.-F. *et al.* Whole-genome sequencing identifies EN1 as a determinant of bone density and fracture. *Nature* **526**, 112–117 (2015).
32. Su, C.-Y. *et al.* Disentangling osteoarthritis-specific genetic effects from obesity to identify novel therapeutic targets. 2025.09.23.25336398 Preprint at https://doi.org/10.1101/2025.09.23.25336398 (2025).
33. Butler-Laporte, G. *et al.* HLA allele-calling using multi-ancestry whole-exome sequencing from the UK Biobank identifies 129 novel associations in 11 autoimmune diseases. *Commun Biol* **6**, 1–17 (2023).
34. Giambartolomei, C. *et al.* Bayesian Test for Colocalisation between Pairs of Genetic Association Studies Using Summary Statistics. *PLOS Genetics* **10**, e1004383 (2014).
35. Zhang, W. *et al.* SharePro: an accurate and efficient genetic colocalization method accounting for multiple causal signals. *Bioinformatics* **40**, btae295 (2024).
36. Leeuw, C. A. de, Mooij, J. M., Heskes, T. & Posthuma, D. MAGMA: Generalized Gene-Set Analysis of GWAS Data. *PLOS Computational Biology* **11**, e1004219 (2015).

37. Finan, C. *et al.* The druggable genome and support for target identification and validation in drug development. *Science Translational Medicine* **9**, eaag1166 (2017).
38. Nilsson, K. H. *et al.* RSPO3 is important for trabecular bone and fracture risk in mice and humans. *Nat Commun* **12**, 4923 (2021).
39. Winkler, D. G. *et al.* Osteocyte control of bone formation via sclerostin, a novel BMP antagonist. *The EMBO Journal* **22**, 6267–6276 (2003).
40. van Bezooijen, R. L. *et al.* Sclerostin Is an Osteocyte-expressed Negative Regulator of Bone Formation, But Not a Classical BMP Antagonist. *J Exp Med* **199**, 805–814 (2004).
41. Stetler-Stevenson, W. G., Krutzsch, H. C. & Liotta, L. A. Tissue Inhibitor of Metalloproteinase (TIMP-2): A new member of the metalloproteinase inhibitor family. *Journal of Biological Chemistry* **264**, 17374–17378 (1989).
42. Page-McCaw, A., Ewald, A. J. & Werb, Z. Matrix metalloproteinases and the regulation of tissue remodelling. *Nat Rev Mol Cell Biol* **8**, 221–233 (2007).
43. Holmbeck, K. *et al.* The metalloproteinase MT1-MMP is required for normal development and maintenance of osteocyte processes in bone. *J Cell Sci* **118**, 147–156 (2005).
44. Holmbeck, K. *et al.* MT1-MMP-Deficient Mice Develop Dwarfism, Osteopenia, Arthritis, and Connective Tissue Disease due to Inadequate Collagen Turnover. *Cell* **99**, 81–92 (1999).
45. Mosig, R. A. *et al.* Loss of MMP-2 disrupts skeletal and craniofacial development and results in decreased bone mineralization, joint erosion and defects in osteoblast and osteoclast growth. *Hum Mol Genet* **16**, 1113–1123 (2007).
46. Inoue, K. *et al.* A Crucial Role for Matrix Metalloproteinase 2 in Osteocytic Canalicular Formation and Bone Metabolism*. *Journal of Biological Chemistry* **281**, 33814–33824 (2006).
47. Martignetti, J. A. *et al.* Mutation of the matrix metalloproteinase 2 gene (MMP2) causes a multicentric osteolysis and arthritis syndrome. *Nat Genet* **28**, 261–265 (2001).
48. Al-Mayouf, S. M., Majeed, M., Hugosson, C. & Bahabri, S. New form of idiopathic osteolysis: Nodulosis, arthropathy and osteolysis (NAO) syndrome. *American Journal of Medical Genetics* **93**, 5–10 (2000).
49. Al Aqeel, A. *et al.* Inherited multicentric osteolysis with arthritis: A variant resembling Torg syndrome in a Saudi family. *American Journal of Medical Genetics* **93**, 11–18 (2000).
50. Rouzier, C. *et al.* A novel homozygous MMP2 mutation in a family with Winchester syndrome. *Clinical Genetics* **69**, 271–276 (2006).
51. Zankl, A., Bonafé, L., Calcaterra, V., Di Rocco, M. & Superti-Furga, A. Winchester syndrome caused by a homozygous mutation affecting the active site of matrix metalloproteinase 2. *Clinical Genetics* **67**, 261–266 (2005).
52. Dew, G. *et al.* Localisation of matrix metalloproteinases and TIMP-2 in resorbing mouse bone. *Cell Tissue Res* **299**, 385–394 (2000).
53. Hill, P. A., Reynolds, J. J. & Meikle, M. C. Inhibition of stimulated bone resorption in vitro by TIMP-1 and TIMP-2. *Biochimica et Biophysica Acta (BBA) - Molecular Cell Research* **1177**, 71–74 (1993).
54. Strongin, A. Y. *et al.* Mechanism Of Cell Surface Activation Of 72-kDa Type IV Collagenase: ISOLATION OF THE ACTIVATED FORM OF THE MEMBRANE METALLOPROTEASE (∗). *Journal of Biological Chemistry* **270**, 5331–5338 (1995).

55. Sobue, T. *et al.* Tissue Inhibitor of Metalloproteinases 1 and 2 Directly Stimulate the Bone-Resorbing Activity of Isolated Mature Osteoclasts. *J Bone Miner Res* **16**, 2205–2214 (2001).
56. Seo, D.-W. *et al.* TIMP-2 disrupts FGF-2-induced downstream signaling pathways. *Microvascular Research* **76**, 145–151 (2008).
57. Seo, D.-W. *et al.* TIMP-2 Mediated Inhibition of Angiogenesis: An MMP-Independent Mechanism. *Cell* **114**, 171–180 (2003).
58. Mi, M. *et al.* TIMP2 deficient mice develop accelerated osteoarthritis via promotion of angiogenesis upon destabilization of the medial meniscus. *Biochemical and Biophysical Research Communications* **423**, 366–372 (2012).
59. Chermside-Scabbo, C. J. *et al.* A proteomics approach to study mouse long bones: examining baseline differences and mechanical loading-induced bone formation in young-adult and old mice. *Aging* **16**, 12726–12768 (2024).
60. Rauner, M. *et al.* Cathepsin S controls adipocytic and osteoblastic differentiation, bone turnover, and bone microarchitecture. *Bone* **64**, 281–287 (2014).
61. Sarma, J. V. & Ward, P. A. New developments in C5a receptor signaling. *CHC* **4**, 73–82 (2012).
62. Morkmued, S. *et al.* Deficiency of the SMOC2 matricellular protein impairs bone healing and produces age-dependent bone loss. *Sci Rep* **10**, 14817 (2020).

Supplementary Figure Legends

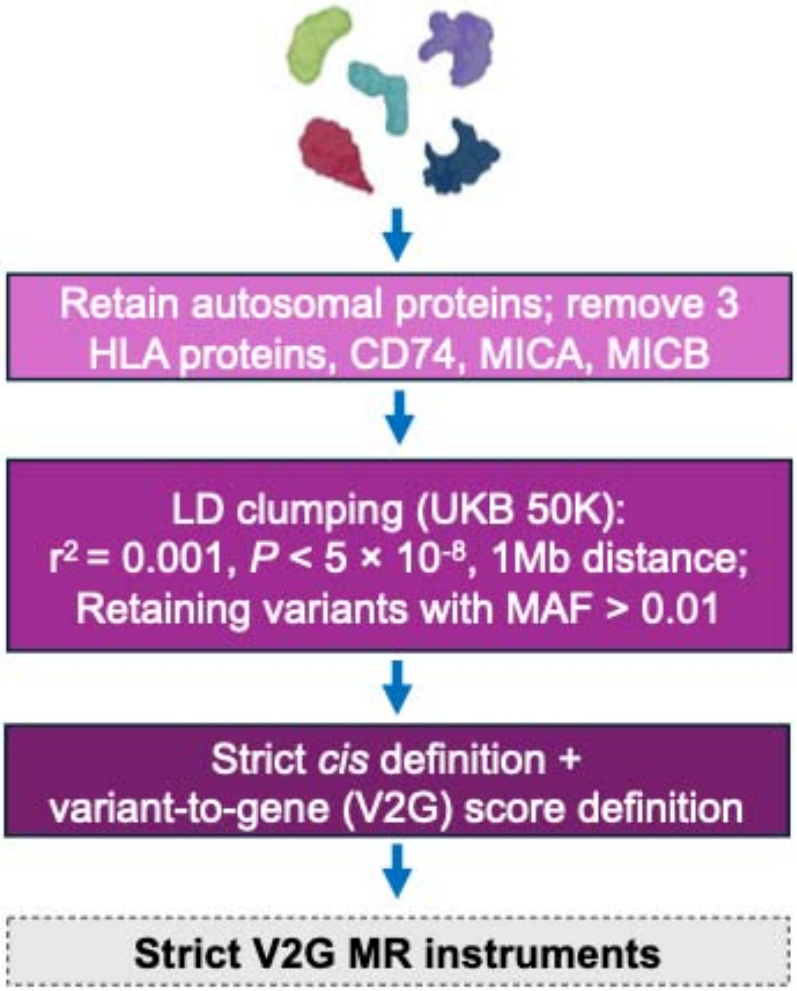

Supplementary Figure 1. Definition and selection of strict variant-to-gene (V2G) *cis*-pQTL instruments for proteome-wide Mendelian randomization (MR). Flowchart summarizing the instrument identification pipeline. For each proteomics cohort, we first retained autosomal proteins and excluded pQTLs mapping to CD74, MICA, and MICB in the HLA region due to complex linkage disequilibrium (LD) and pleiotropy. We then restricted to genome-wide significant *cis*-pQTLs (within 500 kb of the protein-coding gene, $P < 5 \times 10^{-8}$) and performed LD clumping ($r^2 < 0.001$, 1 Mb window) using 50,000 unrelated European individuals from UK Biobank as reference, retaining variants with minor allele frequency > 0.01. Finally, we applied a "strict V2G" filter, keeping only variants that (i) were *cis*-acting on a single protein-coding gene and (ii) had the highest Open Targets Genetics V2G score for that gene. Variants passing all steps comprised the strict V2G *cis*-pQTL used in downstream MR analyses.

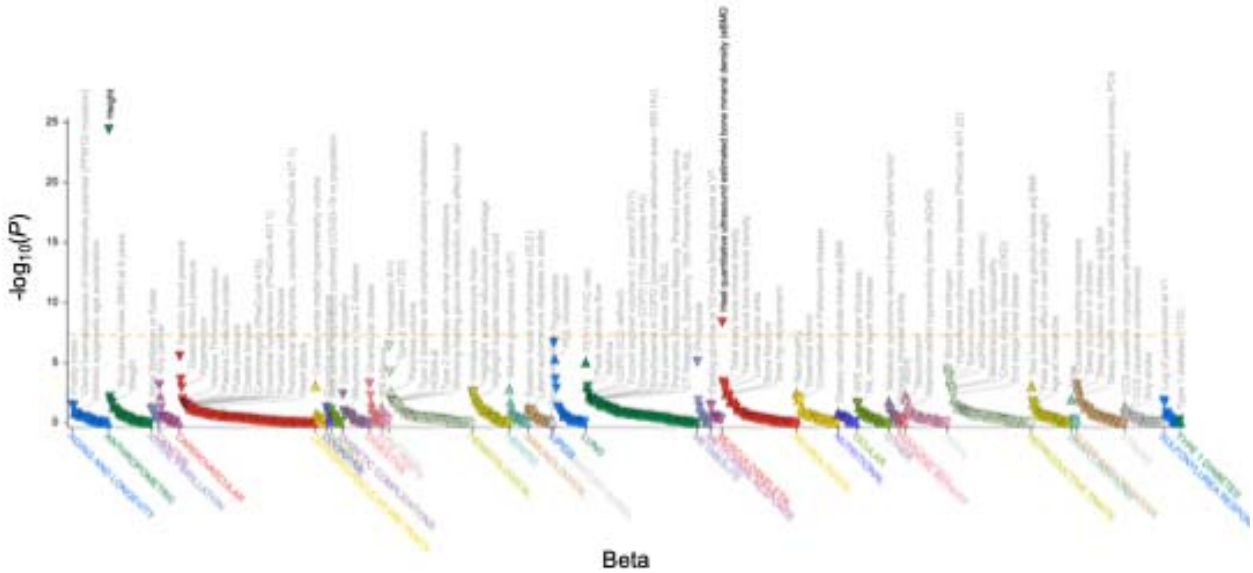

Supplementary Figure 2. Phenome-wide association results for *TIMP2* lead *cis*-pQTL 17:76864175 A>G (rs11077399) in the ARIC cohort.

The plot displays -$\log_{10}$(*P*) for the association between the ARIC lead *cis*-pQTL 17:76864175 A>G (rs11077399) and a broad range of phenotypes in the Association-to-Function (A2F) portal. Triangles denote variant-phenotype associations, grouped by phenotype category on the x-axis and distinguished by color. The y-axis shows -$\log_{10}$(*P*) for the association test. The horizontal orange dashed line indicates the phenome-wide significance threshold used in A2F; points above the line represent associations significant after multiple-testing correction.

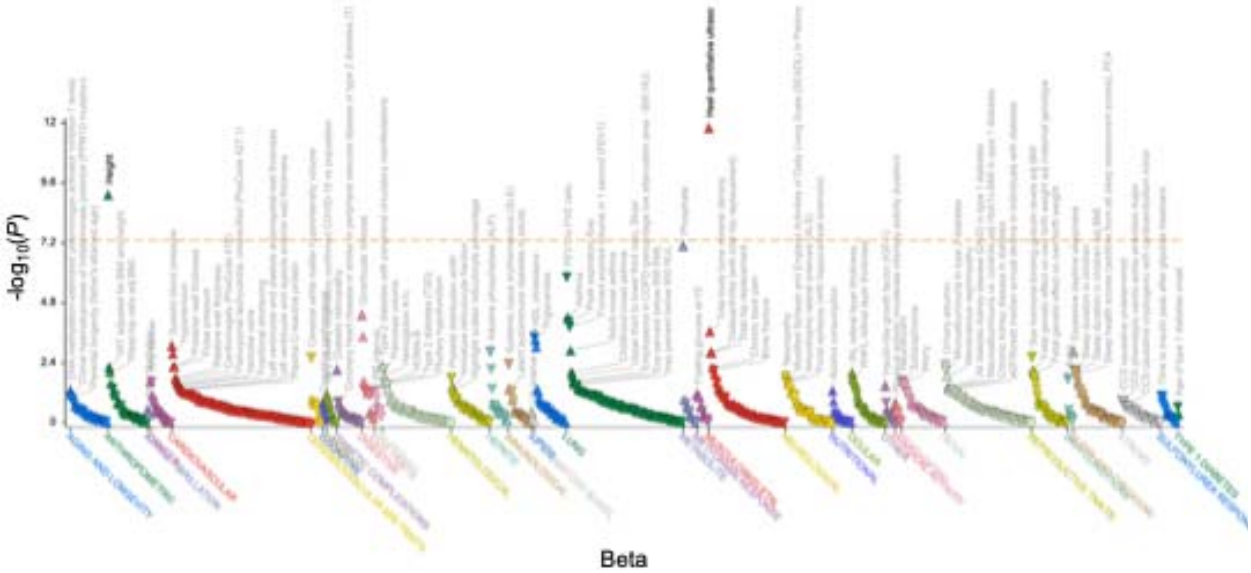

Supplementary Figure 3. Phenome-wide association results for *TIMP2* lead *cis*-pQTL 17:76861940 C>G (rs9894212) in the deCODE cohort.

The plot displays -$\log_{10}(P)$ for the association between the deCODE lead *cis*-pQTL 17:76861940 C>G (rs9894212) and a broad range of phenotypes in the Association-to-Function (A2F) portal. Triangles denote variant-phenotype associations, grouped by phenotype category on the x-axis and distinguished by color. The y-axis shows -$\log_{10}(P)$ for the association test. The horizontal orange dashed line indicates the phenome-wide significance threshold used in A2F; points above the line represent associations significant after multiple-testing correction.

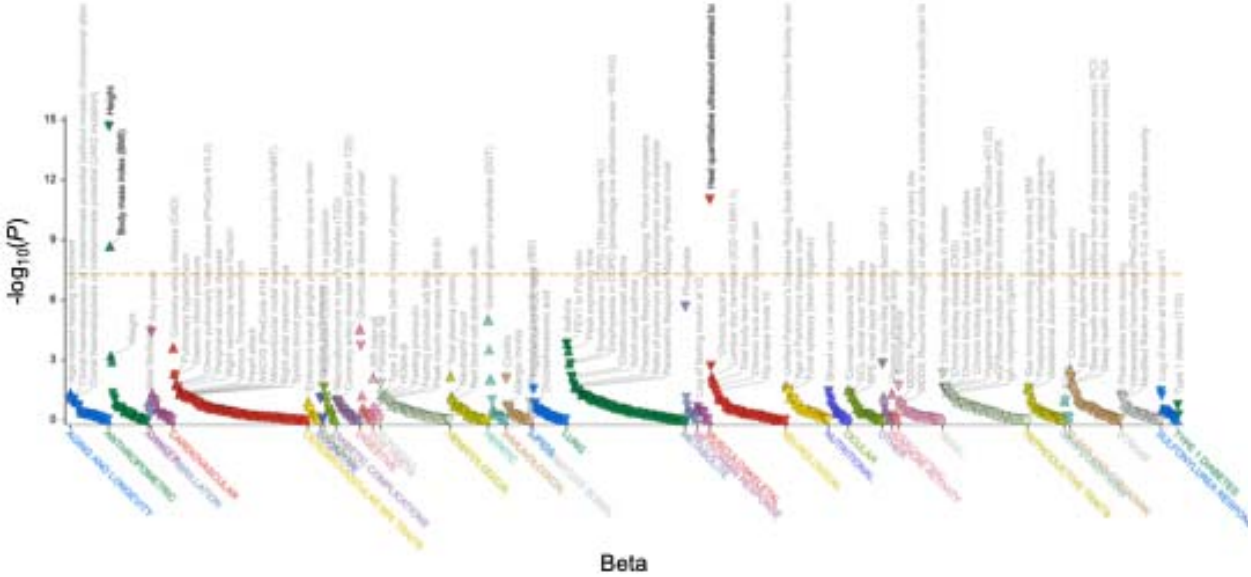

Supplementary Figure 4. Phenome-wide association results for *TIMP2* lead *cis*-pQTL 17:76858539 T>C (rs931227) in the Fenland cohort.

The plot displays -$\log_{10}$(*P*) for the association between the Fenland lead *cis*-pQTL 17:76858539 T>C (rs931227) and a broad range of phenotypes in the Association-to-Function (A2F) portal. Triangles denote variant-phenotype associations, grouped by phenotype category on the x-axis and distinguished by color. The y-axis shows -$\log_{10}$(*P*) for the association test. The horizontal orange dashed line indicates the phenome-wide significance threshold used in A2F; points above the line represent associations significant after multiple-testing correction.

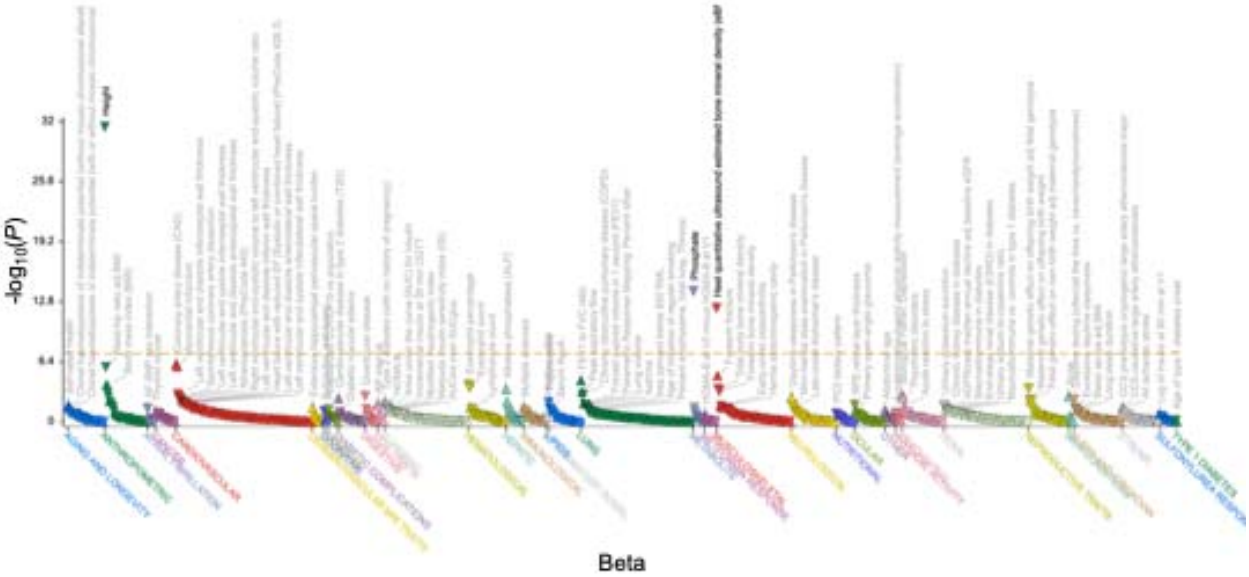

Supplementary Figure 5. Phenome-wide association results for *TIMP2* lead *cis*-pQTL 17:76913843 T>C (rs8066695) in the UKB-PPP cohort.

The plot displays -$\log_{10}(P)$ for the association between the UKB-PPP lead *cis*-pQTL 17:76913843 T>C (rs8066695) and a broad range of phenotypes in the Association-to-Function (A2F) portal. Triangles denote variant-phenotype associations, grouped by phenotype categories on the x-axis and distinguished by color. The y-axis shows -$\log_{10}(P)$ for the association test. The horizontal orange dashed line indicates the phenome-wide significance threshold used in A2F; points above the line represents associations significant after multiple-testing correction.

Figure 1

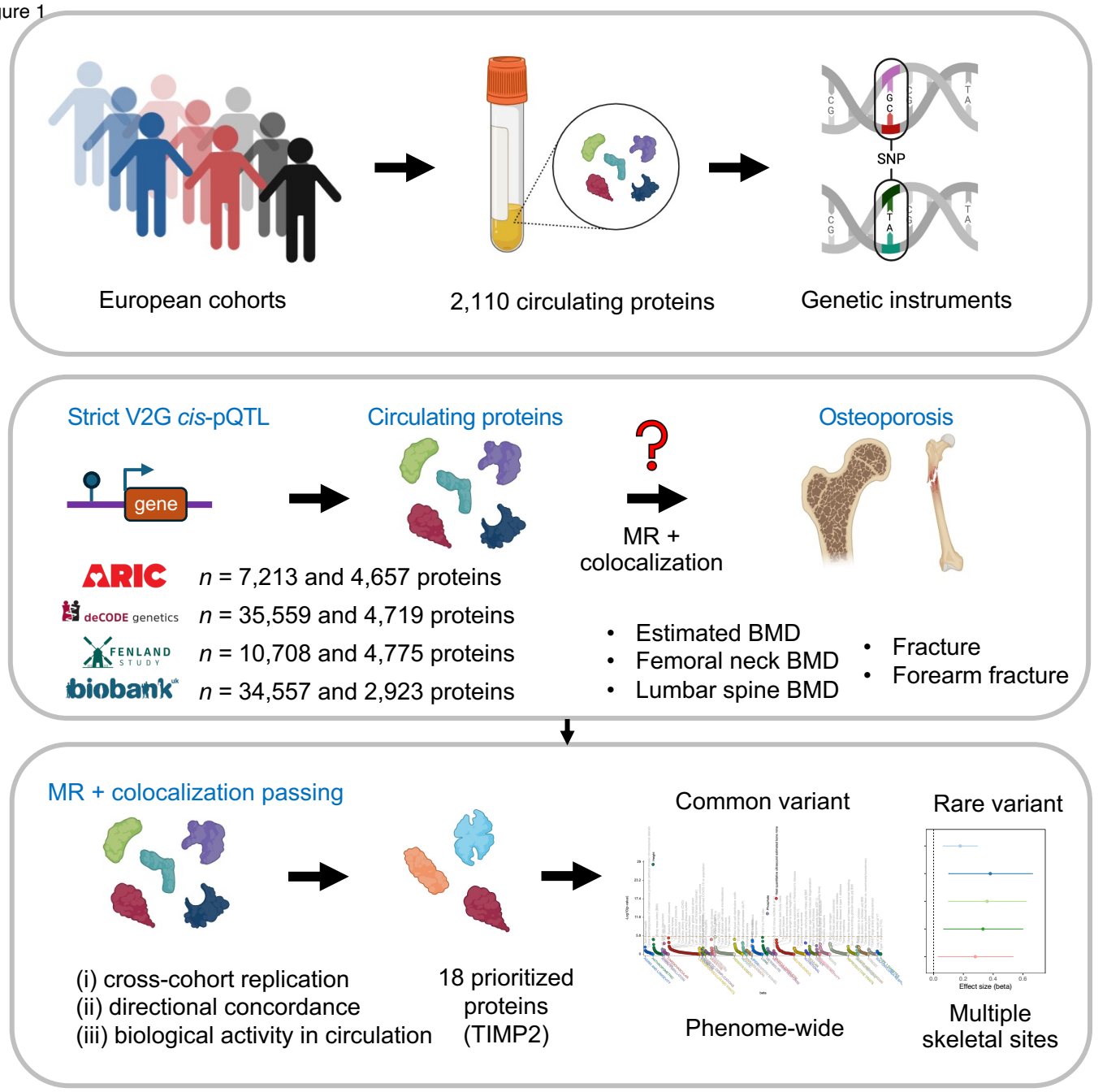

Context of TIMP2 among MR-prioritized proteins

Known

SOST

↑ SOST → ↓ BMD, ↑ fracture
- inhibitor of Wnt/β-catenin
- sclerostin
- romosozumab target

Known

RSPO3

↑ RSPO3 → ↑ BMD, ↓ fracture
- Wnt signaling enhancer

Emerging

TIMP2

↑ TIMP2 → ↓ BMD, ↑ forearm fracture
- ECM/angiogenesis regulator
- secreted MMP inhibitor

Hypothesized mechanism

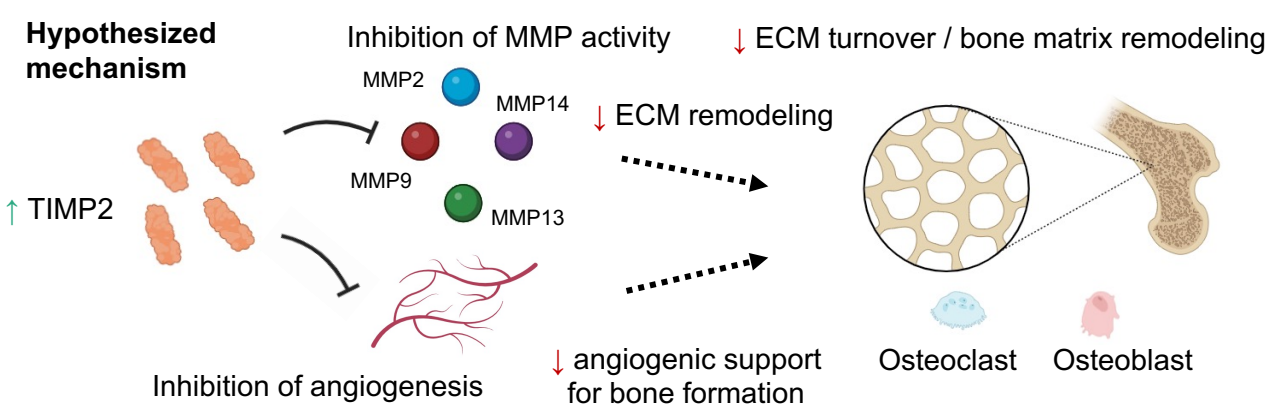

Figure 2

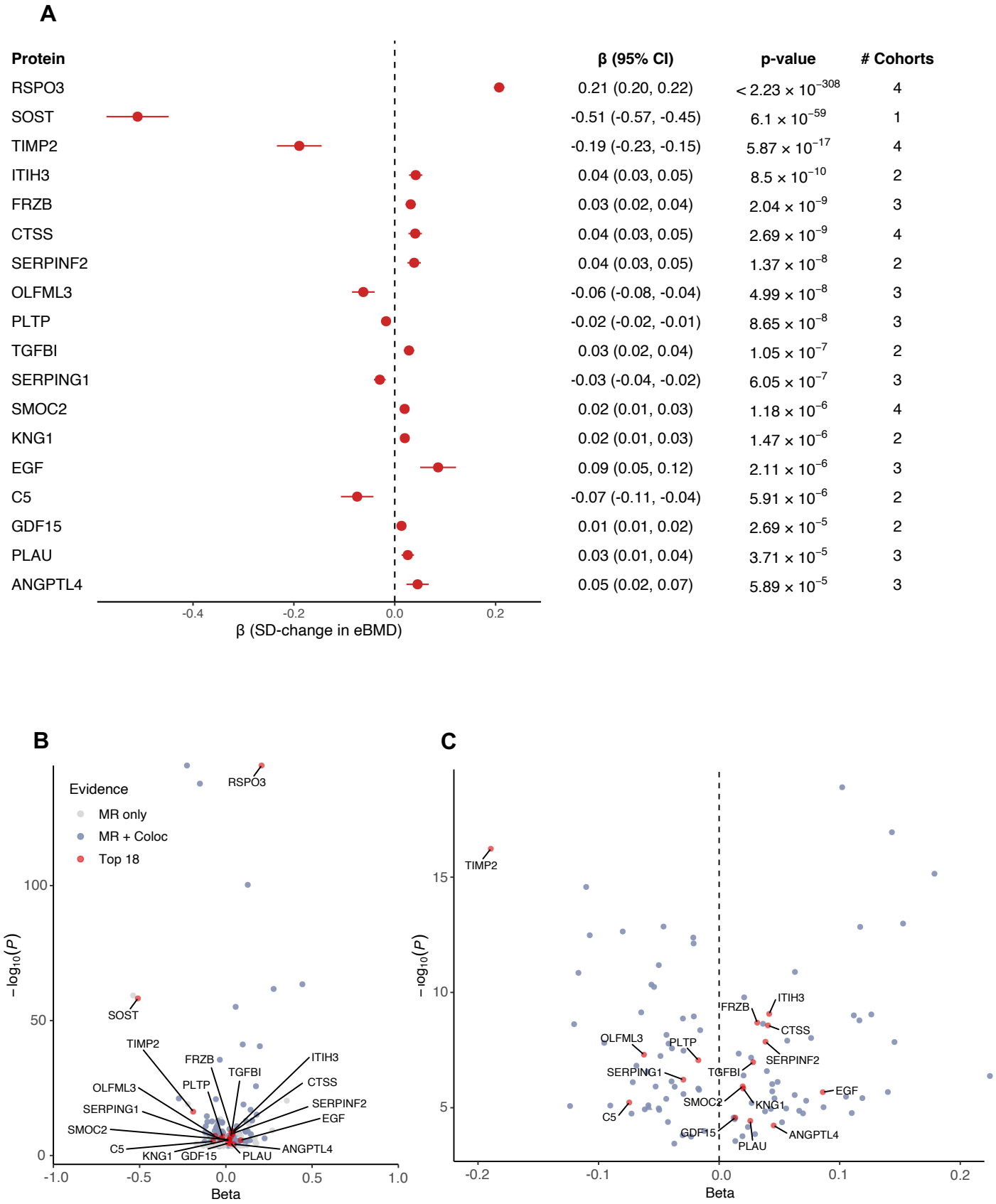
A
Protein
β (95% CI)
p-value
Cohorts
RSPO3 0.21 (0.20, 0.22) < 2.23 × 10^−308 4
SOST -0.51 (-0.57, -0.45) 6.1 × 10^−59 1
TIMP2 -0.19 (-0.23, -0.15) 5.87 × 10^−17 4
ITIH3 0.04 (0.03, 0.05) 8.5 × 10^−10 2
FRZB 0.03 (0.02, 0.04) 2.04 × 10^−9 3
CTSS 0.04 (0.03, 0.05) 2.69 × 10^−9 4
SERPINF2 0.04 (0.03, 0.05) 1.37 × 10^−8 2
OLFML3 -0.06 (-0.08, -0.04) 4.99 × 10^−8 3
PLTP -0.02 (-0.02, -0.01) 8.65 × 10^−8 3
TGFBI 0.03 (0.02, 0.04) 1.05 × 10^−7 2
SERPING1 -0.03 (-0.04, -0.02) 6.05 × 10^−7 3
SMOC2 0.02 (0.01, 0.03) 1.18 × 10^−6 4
KNG1 0.02 (0.01, 0.03) 1.47 × 10^−6 2
EGF 0.09 (0.05, 0.12) 2.11 × 10^−6 3
C5 -0.07 (-0.11, -0.04) 5.91 × 10^−6 2
GDF15 0.01 (0.01, 0.02) 2.69 × 10^−5 2
PLAU 0.03 (0.01, 0.04) 3.71 × 10^−5 3
ANGPTL4 0.05 (0.02, 0.07) 5.89 × 10^−5 3
-0.4
-0.2
0.0
0.2
β (SD-change in eBMD)
B
Evidence
MR only
MR + Coloc
Top 18
RSPO3
SOST
TIMP2
FRZB
TGFBI
ITIH3
OLFML3
PLTP
CTSS
SERPING1
SERPINF2
SMOC2
EGF
C5
KNG1
GDF15
PLAU
ANGPTL4
100
50
0
−log10(P)
-1.0
-0.5
0.0
0.5
1.0
Beta
C
TIMP2
15
10
5
−log10(P)
FRZB
ITIH3
CTSS
OLFML3
PLTP
SERPINF2
SERPING1
TGFBI
EGF
SMOC2
KNG1
C5
GDF15
ANGPTL4
PLAU
-0.2
-0.1
0.0
0.1
0.2
Beta

Figure 3

A

Outcome	Protein	β (95 % CI)	p-value	# Cohorts
Femoral Neck BMD	SOST	-0.59 (-0.81, -0.37)	9.36×10^{-8}	2

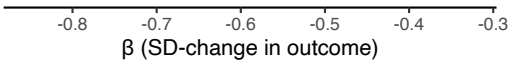

B

Outcome	Protein	Odds ratio (95 % CI)	p-value	# Cohorts
Any Fracture	RSPO3	0.83 (0.80, 0.87)	8.26×10^{-21}	4
	SOST	1.95 (1.62, 2.35)	2.67×10^{-12}	2
Forearm Fracture	RSPO3	0.81 (0.78, 0.83)	9.08×10^{-51}	4
	SOST	2.88 (2.36, 3.53)	6.95×10^{-25}	2
	TIMP2	1.40 (1.20, 1.62)	1.04×10^{-5}	1

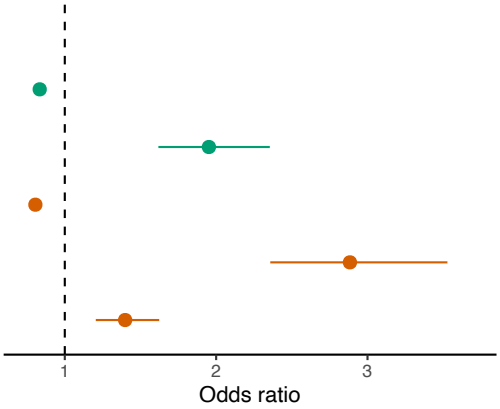

Figure 4

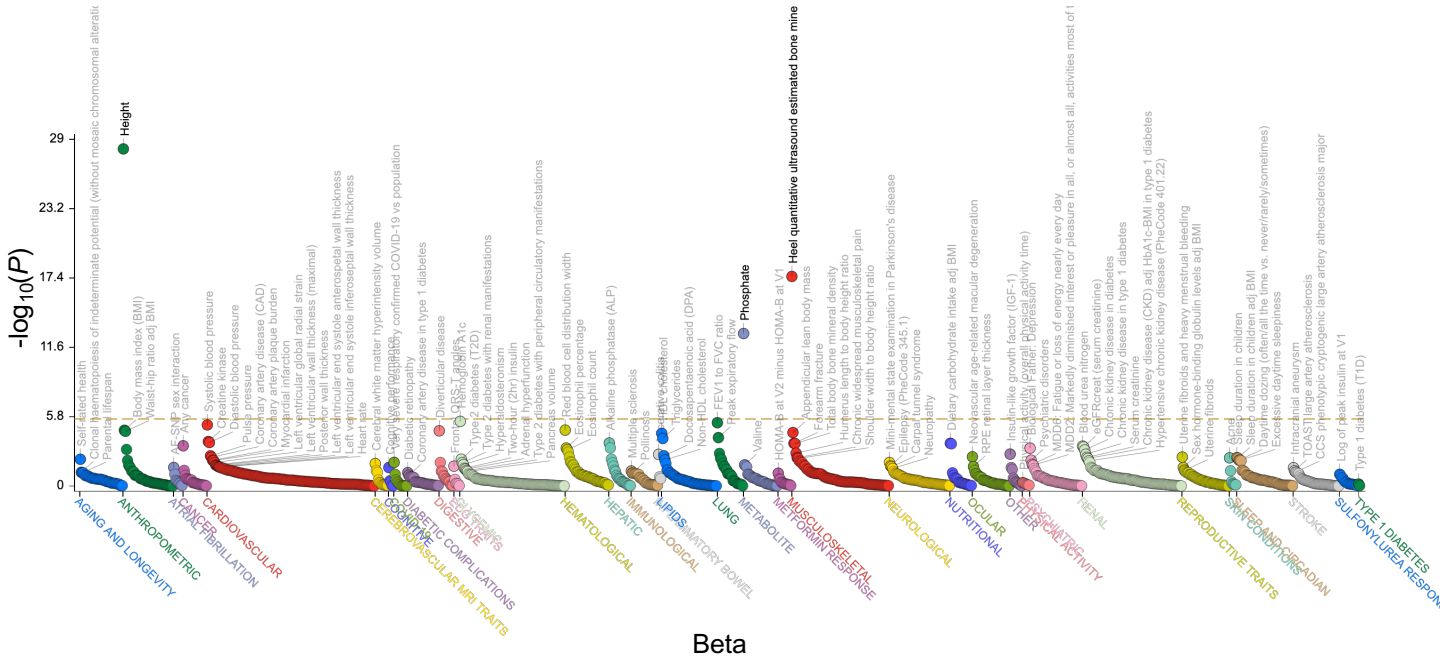
-log10(P)
29
23.2
17.4
11.6
5.8
0
Beta
Height
Heel quantitative ultrasound estimated bone mine
Phosphate
Self-rated health
Clonal haematopoiesis of indeterminate potential (without mosaic chromosomal alteratio
Parental lifespan
Body mass index (BMI)
Waist-hip ratio adj BMI
rs SNP sex interaction
Any cancer
Systolic blood pressure
Creatine kinase
Diastolic blood pressure
Pulse pressure
Coronary artery disease (CAD)
Coronary artery plaque burden
Myocardial infarction
Left ventricular global radial strain
Left ventricular wall thickness (maximal)
Left ventricular end systole anteroseptal wall thickness
Posterior wall thickness
Left ventricular end systole inferoseptal wall thickness
Left atrial volume
Heart rate
Cerebral white matter hyperintensity volume
Cognitive performance
Vary severe respiratory confirmed COVID-19 vs population
Diabetic retinopathy
Coronary artery disease in type 1 diabetes
Diverticular disease
Fronto-temporal lobe
Type 2 diabetes (T2D)
Type 2 diabetes with renal manifestations
Hyperaldosteronism
Two-hour (2hr) insulin
Adrenal hyperfunction
Type 2 diabetes with peripheral circulatory manifestations
Pancreas volume
Red blood cell distribution width
Eosinophil percentage
Eosinophil count
Alkaline phosphatase (ALP)
Multiple sclerosis
Pollinosis
Triglycerides
Docosapentaenoic acid (DPA)
Non-HDL cholesterol
FEV1 to FVC ratio
Peak expiratory flow
Valine
HOMA-B at V2 minus HOMA-B at V1
Appendicular lean body mass
Forearm fracture
Total body bone mineral density
Humerus length to body height ratio
Chronic widespread musculoskeletal pain
Shoulder width to body height ratio
Mini-mental state examination in Parkinson's disease
Epilepsy (PheCode 345.1)
Carpal tunnel syndrome
Neuropathy
Dietary carbohydrate intake adj BMI
Neovascular age-related macular degeneration
RPE retinal layer thickness
Insulin-like growth factor (IGF-1)
Physical activity (overall)
Fatigue
Psychiatric disorders
MDD2 Markedly diminished interest or pleasure in all, or almost all, activities most of t
MDD8 Fatigue or loss of energy nearly every day
Blood urea nitrogen
eGFRcreat (serum creatinine)
Chronic kidney disease in diabetes
Chronic kidney disease in type 1 diabetes
Serum creatinine
Chronic kidney disease (CKD) adj HbA1c-BMI in type 1 diabetes
Hypertensive chronic kidney disease (PheCode 401.22)
Uterine fibroids and heavy menstrual bleeding
Sex hormone-binding globulin levels adj BMI
Uterine fibroids
Acne
Sleep duration in children
Sleep duration in children adj BMI
Daytime dozing (often/all the time vs. never/rarely/sometimes)
Excessive daytime sleepiness
Intracranial aneurysm
TOAST large artery atherosclerosis
CCS phenotypic cryptogenic large artery atherosclerosis major
Log of peak insulin at V1
Type 1 diabetes (T1D)
AGING AND LONGEVITY
ANTHROPOMETRIC
ATRIAL FIBRILLATION
CANCER
CARDIOVASCULAR
CARDIOVASCULAR MRI TRAITS
COGNITIVE
DIABETIC COMPLICATIONS
DIGESTIVE
HEMATOLOGICAL
HEPATIC
IMMUNOLOGICAL
LIPIDS
INFLAMMATORY BOWEL
LUNG
METABOLITE
METFORMIN RESPONSE
MUSCULOSKELETAL
NEUROLOGICAL
NUTRITIONAL
OCULAR
OTHER
PHYSICAL ACTIVITY
PSYCHIATRIC
RENAL
REPRODUCTIVE TRAITS
SKIN CONDITIONS
SLEEP AND CIRCADIAN
STROKE
SULFONYLUREA RESPONS
TYPE 1 DIABETES

Figure 5

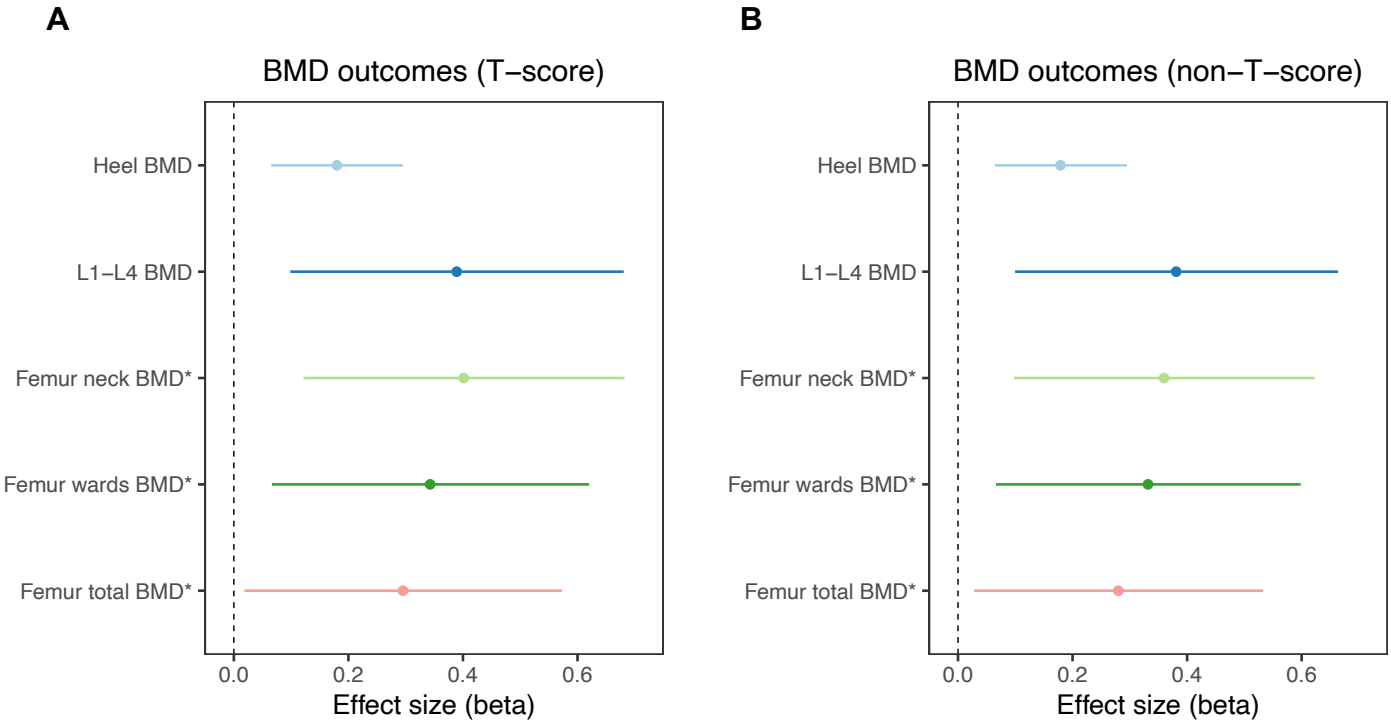
A
BMD outcomes (T−score)
Heel BMD
L1−L4 BMD
Femur neck BMD*
Femur wards BMD*
Femur total BMD*
0.0
0.2
0.4
0.6
Effect size (beta)
B
BMD outcomes (non−T−score)
Heel BMD
L1−L4 BMD
Femur neck BMD*
Femur wards BMD*
Femur total BMD*
0.0
0.2
0.4
0.6
Effect size (beta)

Figure 6

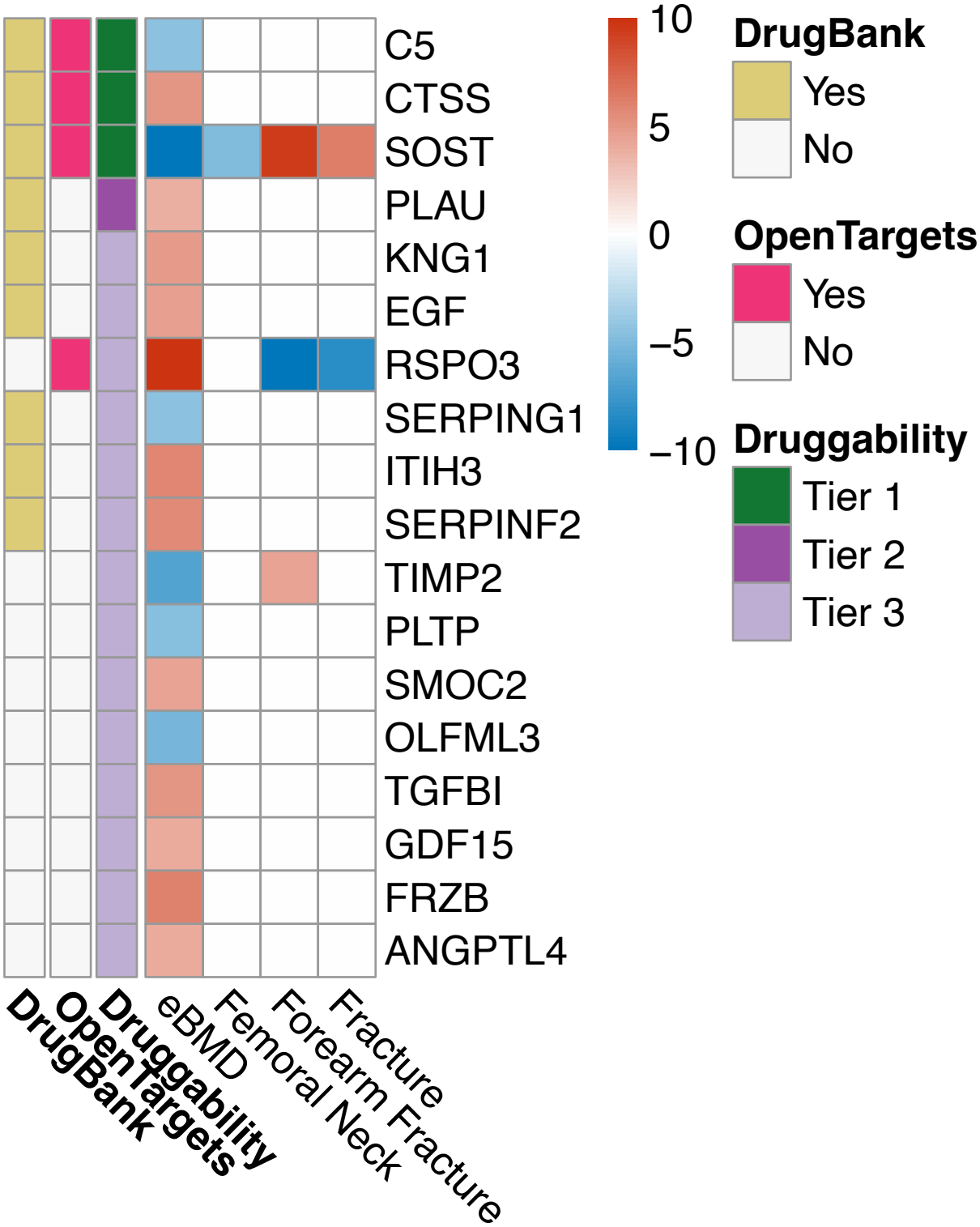
C5
CTSS
SOST
PLAU
KNG1
EGF
RSPO3
SERPING1
ITIH3
SERPINF2
TIMP2
PLTP
SMOC2
OLFML3
TGFBI
GDF15
FRZB
ANGPTL4
DrugBank
OpenTargets
Druggability
eBMD
Femoral Neck
Forearm Fracture
Fracture
10
5
0
−5
−10
DrugBank
Yes
No
OpenTargets
Yes
No
Druggability
Tier 1
Tier 2
Tier 3

Supplementary Figure 1

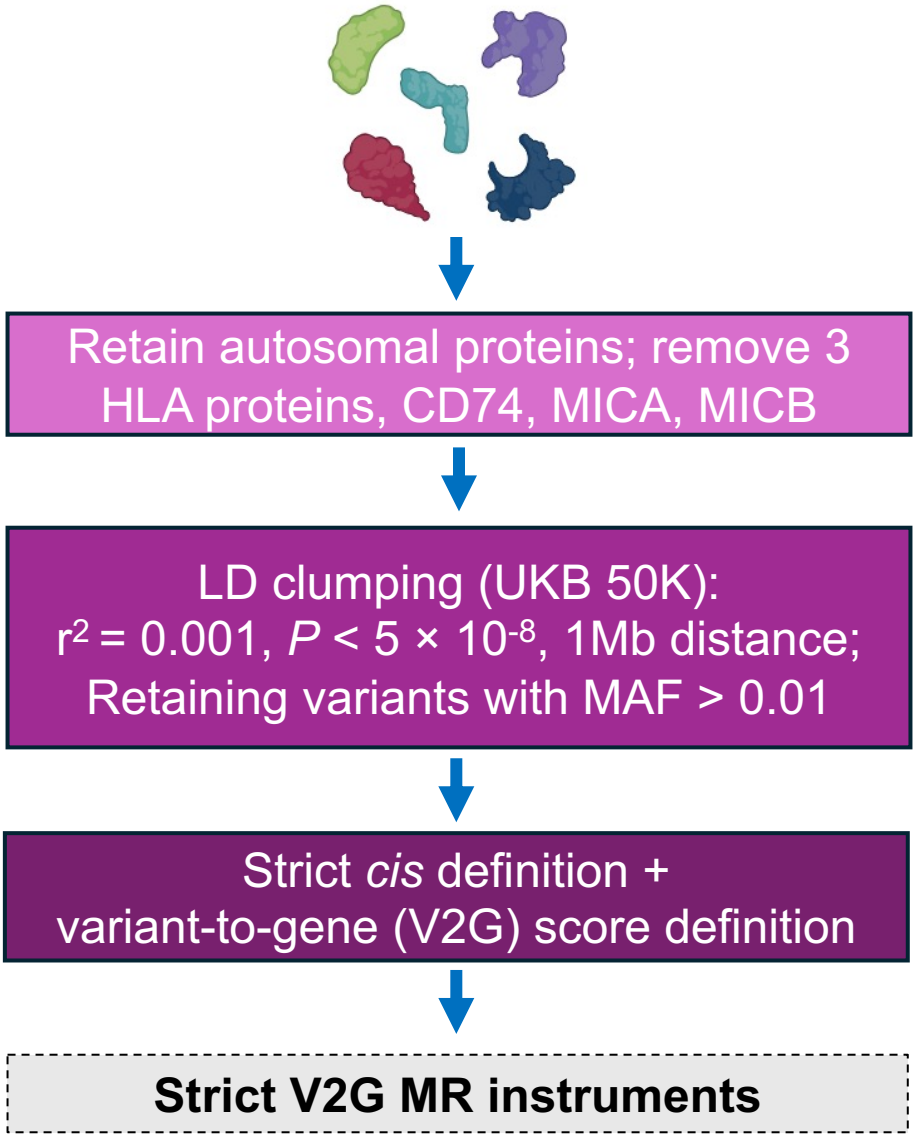

Supplementary Figure 2

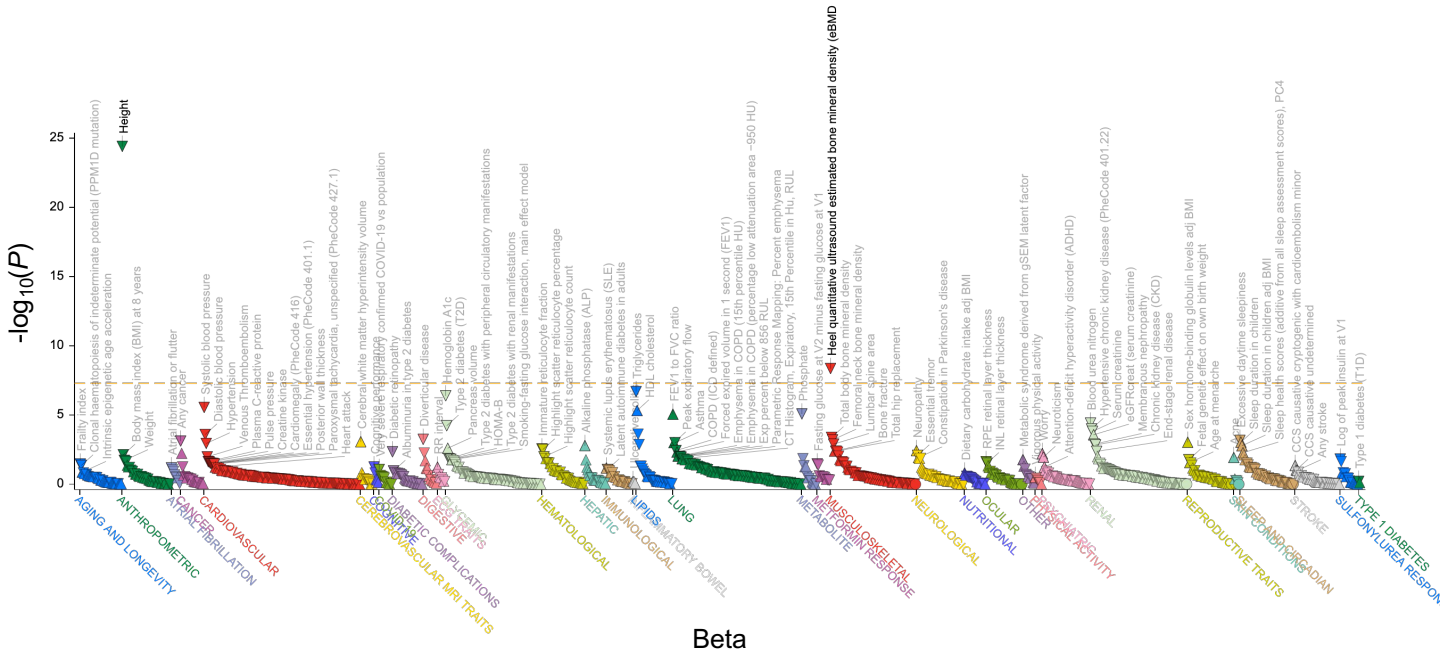

Supplementary Figure 3

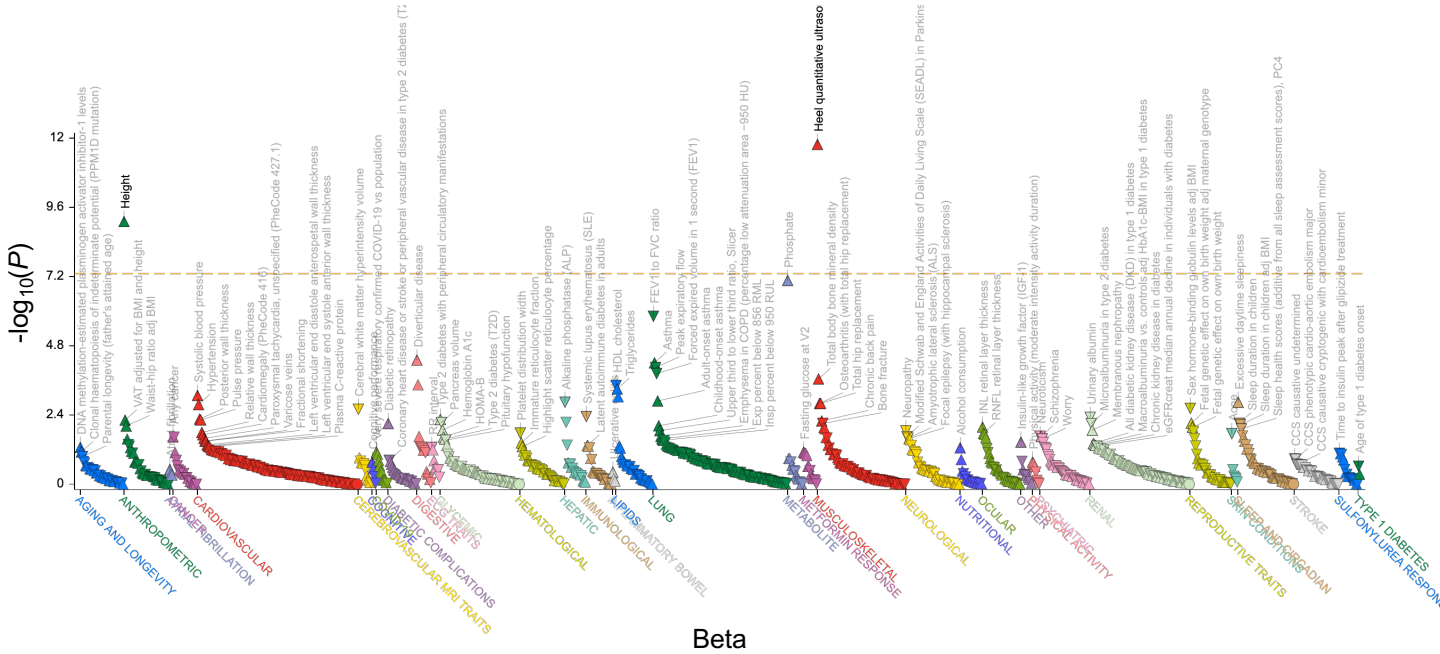

Supplementary Figure 4

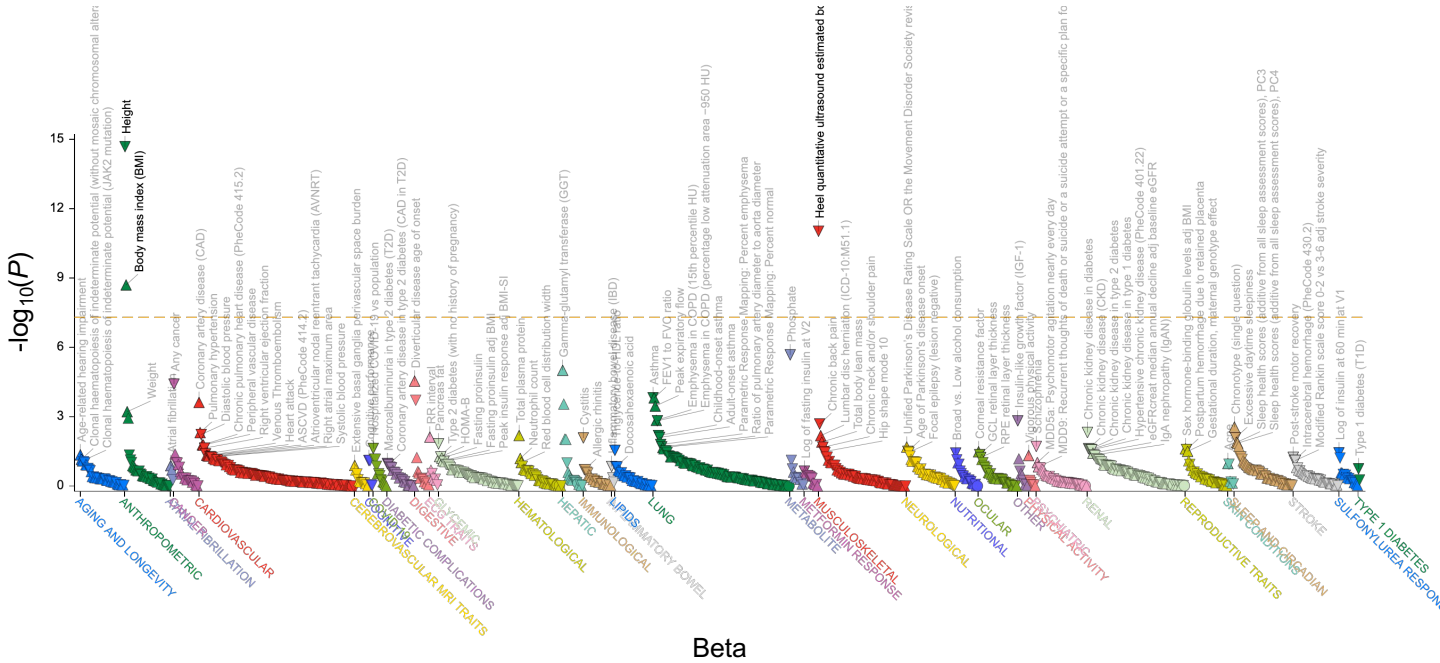
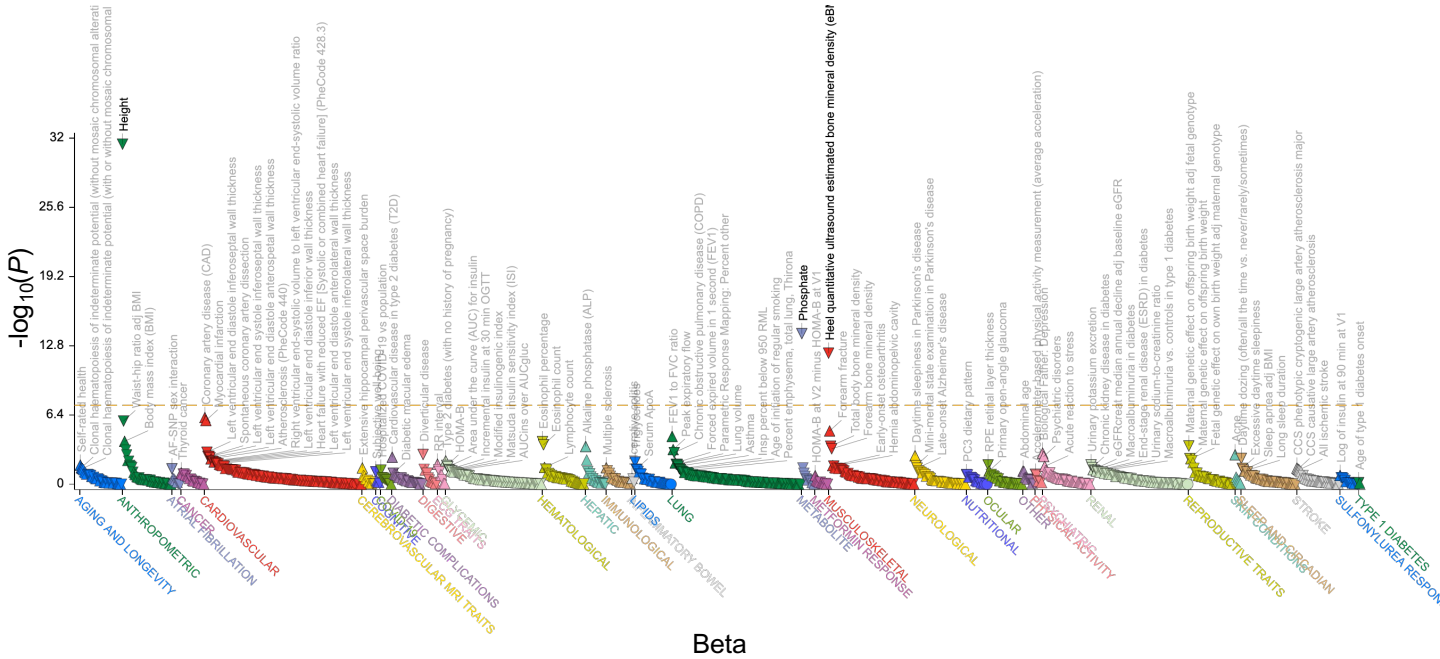
Supplementary Figure 5